

NASA TECHNICAL NOTE



NASA TN D-2133

C.1

NASA TN D-2133

LOAN COPY: RETURN
AFWL (WLL—)
KIRTLAND AFB, N ME



**LARGE-SCALE WIND-TUNNEL TESTS
OF AN AIRPLANE MODEL
WITH AN UNSWEPT TILT WING
OF ASPECT RATIO 5.5, AND
WITH VARIOUS STALL CONTROL DEVICES**

by James A. Weiberg and Demo J. Giulianetti

*Ames Research Center
Moffett Field, California*

LARGE-SCALE WIND-TUNNEL TESTS OF AN AIRPLANE MODEL
WITH AN UNSWEPT TILT WING OF ASPECT RATIO 5.5,
AND WITH VARIOUS STALL CONTROL DEVICES

By James A. Weiberg and Demo J. Giulianetti

Ames Research Center
Moffett Field, Calif.

NATIONAL AERONAUTICS AND SPACE ADMINISTRATION

For sale by the Office of Technical Services, Department of Commerce,
Washington, D.C. 20230 -- Price \$1.25



LARGE-SCALE WIND-TUNNEL TESTS OF AN AIRPLANE MODEL

WITH AN UNSWEPT TILT WING OF ASPECT RATIO 5.5,

AND WITH VARIOUS STALL CONTROL DEVICES

By James A. Weiberg and Demo J. Giulianetti

SUMMARY

Results are presented of the effects of slats, flaps, wing-fuselage ramp fairing, and propeller rotation on the flow separation, buffet, and descent characteristics of a tilt-wing deflected-slipstream VTOL model. The results indicated that wing stall and resulting buffet in descending flight could be delayed approximately 15 knots by a slat, BLC nose flap, or increased trailing-edge flap effectiveness.

INTRODUCTION

The tests reported in reference 1 indicated that there would be a problem of attaining descent rates of the order of 500 feet per minute at low speed without buffeting. The buffeting was produced by air-flow separation from the center section of the tilted wing which was not immersed in the propeller slipstream. To determine the extent to which this separation could be contained or delayed, tests were made of the model with various leading-edge flaps and slats and a fairing between the tilted wing and fuselage. To determine the magnitude of the buffeting, the oscillatory force at the model support points and accelerations in the model structure were measured. The results of these tests are presented herein.

NOTATION

- b wing span, ft
 c wing chord parallel to plane of symmetry, ft
 \bar{c} mean aerodynamic chord, $\frac{2}{S} \int_0^{b/2} c^2 dy$, ft
 C_D drag coefficient including thrust, $\frac{\text{measured drag}}{q_\infty S}$
 C_L lift coefficient, $\frac{\text{lift}}{q_\infty S}$
 C_l rolling-moment coefficient, $\frac{\text{rolling moment}}{q_\infty S b}$
 C_m pitching-moment coefficient, $\frac{\text{pitching moment}^1}{q_\infty S}$

¹Moments are presented about the center shown in figure 2(d).

- C_n yawing-moment coefficient, $\frac{\text{yawing moment}}{q_\infty S b}$
 C_Y side-force coefficient, $\frac{\text{side force}}{q_\infty S}$
 C_μ jet momentum coefficient, $\frac{w_j}{g q_\infty S} V_j$
 g acceleration of gravity, 32.2 ft/sec²
 i_t angle of stabilizer relative to fuselage reference line, deg
 J propeller advance ratio, $\frac{V_\infty}{nD}$
 n propeller angular velocity, rps
 D propeller diameter, ft
 p_∞ free-stream static pressure, lb/sq ft
 p_d' total pressure in flap duct, lb/sq ft
 q_∞ free-stream dynamic pressure, lb/sq ft
 R gas constant for air, 1715 ft²/sec² °R
 S wing area, sq ft
 T_d duct temperature, °R
 T_c' thrust coefficient, $\frac{\text{thrust}}{q_\infty S}$
 V_j jet velocity for isentropic expansion $\sqrt{\frac{2\gamma}{\gamma-1} RT_d \left[1 - \left(\frac{p_\infty}{p_d'} \right)^{\frac{\gamma-1}{\gamma}} \right]}$, fps
 V_∞ free-stream velocity, fps
 w_j weight rate of air flow through nozzle, lb/sec
 y spanwise distance, perpendicular to plane of symmetry, ft
 α angle of attack of fuselage reference line, deg
 β sideslip angle, deg
 δ_f flap deflection measured in plane normal to flap hinge line, deg
 δ_w wing tilt measured from a wing-down position having 8.3° incidence of the root chord with respect to the fuselage reference line, deg
 γ ratio of specific heats (1.4 for air), and glide angle, deg

Subscripts

- f trailing-edge flap
n BLC nose flap

MODEL AND APPARATUS

The model for these tests is shown in figure 1 and was the same model used in reference 1. The wing could be tilted 20° , 30° , and 50° from a wing-down position at which the incidence of the root chord was 8.3° with respect to the fuselage reference line. Except where noted on the figures, all the tests were made with the vertical tail off and the horizontal tail at 14° incidence to the fuselage reference line. The geometry of the model and details of the stall control devices are shown in table I and in figure 2. The stall control devices consisted of a leading-edge slat (fig. 2(b)), a BLC nose flap (fig. 2(b)), and a ramp-type fairing between the fuselage and the leading-edge of the tilted wing (fig. 2(c)). This latter ramp-type fairing will be referred to as the ramp. For some tests, only the portion of the ramp aft of the wing leading edge was tested. This portion of the ramp will be referred to as the aft ramp. The BLC nose flap completely spanned the wing. The various spanwise extents of slats tested are shown in figure 2(b). The full-span slat extended over the fuselage with the wing tilted and ended at the side of the fuselage with the wing down.

The blowing boundary-layer-control system used on the flaps is described in reference 2. The height of the jet nozzle was 0.060 inch on the trailing-edge flaps and 0.080 inch on the leading-edge flaps. The momentum flow coefficient, C_μ , used on the flaps was above the critical value defined as the minimum flow coefficient above which little or no change in lift occurred. For the trailing-edge flaps this value was determined from the data presented in reference 2. For the BLC nose flap, the critical C_μ was determined from the data in figure 3. The model was equipped with 4 three-bladed propellers. The geometric characteristics of these propellers are given in reference 3. The blade angle at 0.75 blade radius was 21.5° . The majority of the data was obtained with the propellers rotating in the direction shown in figure 2(a) and, unless noted, the data presented were with this rotation.

Tests were made at free-stream velocities from 0 to 93 fps ($q_\infty = 10$ and a Reynolds number of 2.8 million based on the wing mean aerodynamic chord of 5.18 feet). The data presented in the figures include the direct propeller forces as well as the aerodynamic forces. The propeller thrust characteristics for 0° wing tilt are given in reference 1 and are felt to be sufficiently accurate for all the tilt angles tested based on the data in reference 4.

Moments are presented about the center shown in figure 2(d).

Tunnel-wall corrections were not applied to any of the data.

Measurements of the stall buffet intensity were made using the output from strain-gage-type load cells mounted between the model and the support struts and from accelerometers located in the model structure. These data were recorded on an oscillograph.

RESULTS AND DISCUSSION

The basic lift, drag, and pitching-moment characteristics of the model are presented in figures 4 to 9. Data are presented for flap deflections of 0°, 30°, 50°, and 80°, wing tilt angles of 0°, 20°, 30°, and 50°, and thrust coefficients T_c' from 0 to 4. The corresponding figures for these configurations are listed in the following table together with the device used to control wing stall.

δ_f	δ_w	Stall control device	Figure
0	0	None	4
30	0	None	5(a)
30	0	Full-span slat	5(b)
50	0	Full-span slat	5(c)
80	0	Full-span slat	5(d)
30	20	None	6(a)
30	20	Full-span slat	6(b)
30	30	None	7(a)
30	30	Wing-fuselage ramp fairing	7(b)
30	30	Center slat	7(c)
30	30	Outboard slat with ramp	7(d)
30	30	Full-span slat	7(e)
30	30	Full-span slat with ramp	7(f)
30	30	BLC nose flap with ramp	7(g)
30	30	BLC nose flap with aft ramp	7(h)
50	30	BLC nose flap	8
30	50	Full-span slat	9

Effect of Stall Control Devices on Stall and Buffet

Tuft studies showed that with the wing tilted, flow separation originated on the wing center section over the fuselage and on an area between the nacelles on each wing panel (fig. 10). From these areas the separation spread spanwise with increasing angle of attack. The flow separation in these areas was delayed to higher angles of attack by either the full-span slat or the BLC nose flap which extended over the entire wing span (including that part of the tilted wing above the fuselage).

In addition, the full-span slat and the BLC nose flap increased maximum lift and the angle-of-attack for maximum lift (e.g., see figs. 5(a) and (b); 6(a) and (b); 7(a), (e), (f), (g)). A slat over only the center section between the

inboard nacelles did not noticeably alter the flow separation in this region nor provide any increase in lift (cf. figs. 7(a) and (c)). With the ramp fairing between the fuselage and the tilted wing but with no leading-edge device, flow separation started in the area between the nacelles on each wing panel and progressed spanwise until it had spread onto the rear portion of the aft ramp. The aft ramp alone was as effective as the complete ramp in delaying the center section stall (cf. figs. 7(g) and (h)). The ramp did not alter the steady force characteristics but did delay the onset of tail buffet due to flow separation from the wing.

The flow separation and stall were accompanied by buffeting of the model. Measurements were made of the magnitude of the fluctuating forces involved. These fluctuations were random in magnitude as shown by the typical oscillograph traces in figure 11. The frequency of the oscillations corresponded to the natural frequency of the model structure. The maximum peak-to-peak fluctuations were measured from traces such as those in figure 11. The variations with angle of attack of half of the peak-to-peak value of these fluctuations for some of the configurations tested are shown in figures 12 and 13. The stall buffet intensities shown were measured with an accelerometer on the tip of the horizontal tail and from a load cell on one of the model support struts. The accelerations were measured perpendicular to the horizontal-tail plane and the oscillating forces, perpendicular to the wing reference plane. These data are for a free-stream dynamic pressure of 10 psf. From these data, the angle of attack for the start of buffet rise was obtained and is shown in the basic force data of figures 4 to 9 by a shaded symbol. For the plain wing, flow separation accompanied by buffet rise usually preceded $C_{L_{max}}$, but was not necessarily accompanied by an abrupt change in force characteristics. In general, the slat, BLC nose flap, and ramp configurations delayed flow separation and accompanying buffet to higher angles of attack so that the buffet rise more nearly coincided with $C_{L_{max}}$.

Effect of Stall Control Devices on Operational Characteristics

Flight tests of a tilt-wing airplane (ref. 5) have shown that the wing stall and separation (ref. 6) which occurs in a descent or a decelerating conversion leads to buffeting and erratic motions with general difficulty in handling the aircraft. For the present model, the effects of the various stall control devices on the descent characteristics in the transition were estimated. Glide angles were computed from the data in figures 4 to 9 for an airplane having a wing loading of 50 psf. Results are presented in figures 14 for two configurations showing the variation of glide angle throughout an angle of attack and thrust coefficient range. Boundaries of stall buffet rise and $\pm 15^\circ$ angle of attack are shown on these figures. The stall boundary defines, for a given velocity, the glide angle above which a rise in the buffet magnitude was indicated from the measured fluctuating forces. This boundary was determined using data similar to that in figures 12 and 13. Boundaries for stall buffet rise for the various configurations tested are compared in figures 15 to 18. As an indication of the descent rates attained with these glide angles, a curve showing the glide angle for 500 fpm descent is included on the figures. Flap deflection, wing-fuselage ramp fairing, slats, and BLC nose flaps all increased the value of

buffet-free glide angle at a given speed. All but flap deflection provided this increased glide angle as a result of delay in angle of attack before buffet. Change in propeller rotation from right hand (used in ref. 1) to that shown in figure 2, reduced the center section stall with a subsequent increase in the glide angle before buffet (see fig. 17). Some data were also obtained with the inboard propellers interchanged to give down-going blades between the propellers. This configuration alleviated flow separation between the nacelles on each wing panel but worsened the center section stall. This interchange of propeller rotation did not alter the steady force characteristics but did reduce the glide angle before buffet.

Although most of these stall control devices provided sizable improvements in the descent capability, descent rates greater than 500 fpm could not be obtained at speeds below 40 knots without buffet even with the best configuration. The best configuration investigated was blowing BLC trailing-edge flaps deflected 50° with full-span leading-edge slats or BLC nose flap, counterrotating propellers and wing-fuselage ramp fairing.

Lateral-Directional Characteristics

The characteristics of the model in sideslip are shown in figure 19 for 0° wing tilt and flaps 0° and 50° with the vertical tail on, and 4° horizontal-tail incidence. No lateral-directional data were obtained on this model with all the propellers rotating in the same direction. However, comparisons with data from reference 3 on the aspect ratio 10 wing (from which the present model was made by cutting off the tips), indicate that, as expected, propeller rotation has a large effect on lateral-directional characteristics. The counterrotating propeller arrangement of the present tests eliminated or greatly reduced the large effects of power on $C_{n\beta}$ and $C_{l\beta}$; the large variation of C_y with angle of attack (fig. 20) was also essentially eliminated. This latter large variation of side force with angle of attack was shown to impair the airplane's handling qualities (ref. 7) but it is not necessarily typical of multiengine propellered airplanes (ref. 8).

CONCLUDING REMARKS

The wind-tunnel tests showed that maximum lift of the tilt-wing deflected slipstream VTOL model was limited by separation from the center section of the wing outside the slipstream and from an area between the nacelles. High-lift trailing-edge flaps and powerful leading-edge stall control devices delayed this separation so that some descent capability could be obtained without buffet in the transition speed range. It was shown that propeller rotation had a large influence on wing flow separation and on lateral and directional characteristics.

Ames Research Center
National Aeronautics and Space Administration
Moffett Field, Calif., Oct. 28, 1963.

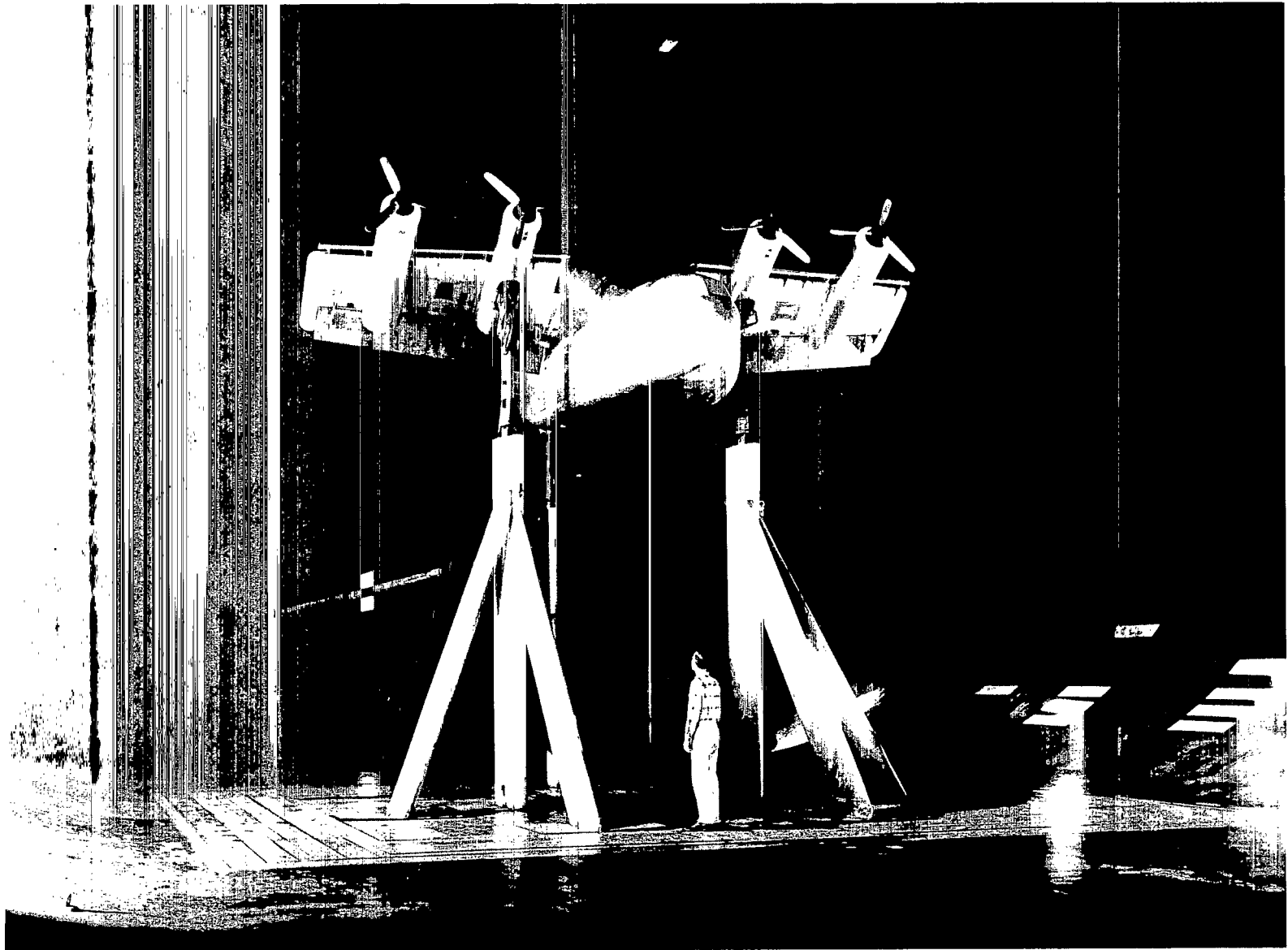
REFERENCES

1. Weiberg, James A., and Holzhauser, Curt A.: Large-Scale Wind-Tunnel Tests of an Airplane Model With an Unswept, Tilt Wing of Aspect Ratio 5.5, and With Four Propellers and Blowing Flaps. NASA TN D-1034, 1961.
2. Griffin, Roy N., Jr., Holzhauser, Curt A., and Weiberg, James A.: Large-Scale Wind-Tunnel Tests of an Airplane Model With an Unswept, Aspect-Ratio-10 Wing, Two Propellers, and Blowing Flaps. NASA MEMO 12-3-58A, 1958.
3. Weiberg, James A., and Page, V. Robert: Large-Scale Wind-Tunnel Tests of an Airplane Model With an Unswept, Aspect-Ratio-10 Wing, Four-Propellers, and Blowing Flaps. NASA TN D-25, 1959.
4. Yaggy, Paul F., and Ragallo, Vernon L.: A Wind-Tunnel Investigation of Three Propellers Through and Angle-of-Attack Range from 0° to 85° , NASA TN D-318, 1960.
5. Pegg, Robert J.: Summary of Flight-Test Results of the VZ-2 Tilt-Wing Aircraft. NASA TN D-989, 1962.
6. Mitchell, Robert G.: Full-Scale Wind-Tunnel Test of the VZ-2 VTOL Airplane with Particular Reference to the Wing Stall Phenomena. NASA TN D-2013, 1963.
7. Innis, Robert C., and Quigley, Hervey C.: A Flight Examination of Operating Problems of V/STOL Aircraft in STOL-Type Landing and Approach. NASA TN D-862, 1961.
8. Quigley, Hervey C., and Innis, Robert C.: Handling Qualities and Operational Problems of a Large-Four-Propeller STOL Transport Airplane. NASA TN D-1647, 1963.

TABLE I.- GENERAL GEOMETRIC DIMENSIONS OF THE MODEL

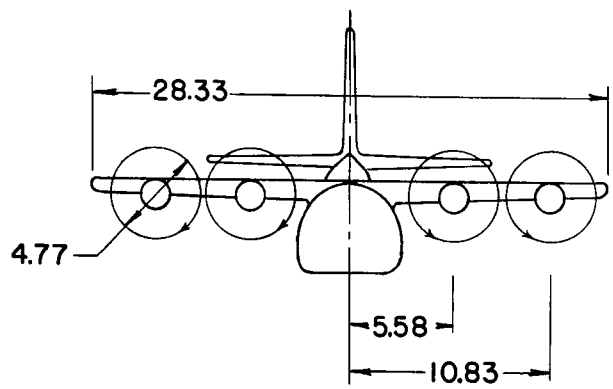
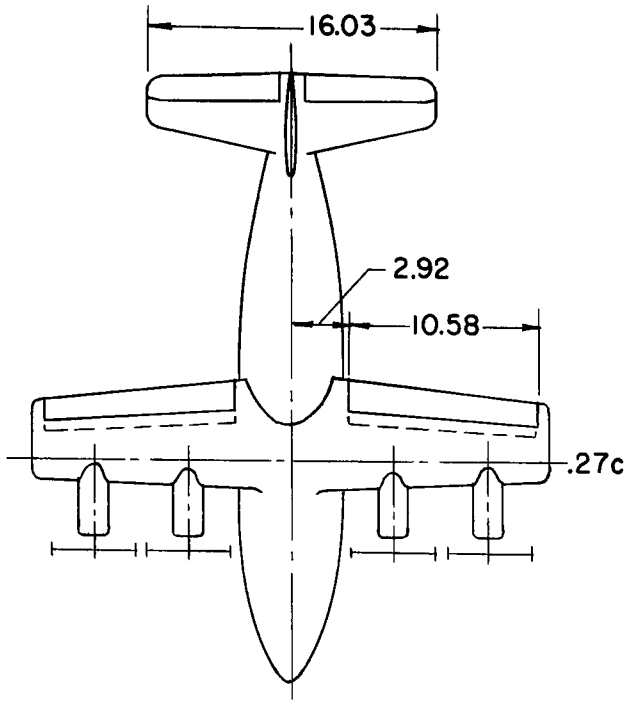
Dimension	Wing	Horizontal surface	Vertical surface
Area, sq ft	145.0	56.5	30.6
Span, ft	28.33	16.03	7.19
\bar{c} , ft	5.18	3.50	4.68
Aspect ratio	5.54	4.55	1.69
Taper ratio	.69	.45	.55
Geometric twist, deg	2.2 ⁰	0	0
	(washout)		
Dihedral from reference plane, deg	0.8	0	--
Incidence from reference plane, 0° tilt, deg	8.3	--	--
Section profile (constant)	NACA 23017	NACA 0012	NACA 0012
Root chord, ft	6.07	4.61	5.88
Tip chord, ft	4.18	2.54	2.65
Sweep of leading edge, deg	2	12	24
Tail length, ft	--	18.03 ^a	--

^aDistance from 0.25 \bar{c} of wing to 0.25 \bar{c} of horizontal tail, 0° wing tilt.

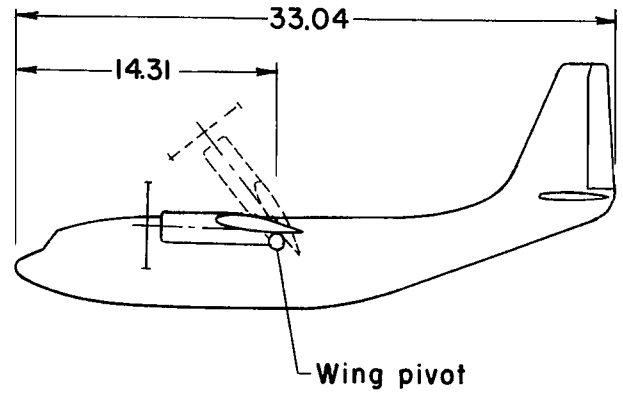


A-28169

Figure 1.- The model with slats and wing-fuselage ramp fairing mounted in the wind tunnel; $\delta_f = 50^\circ$,
 $\delta_w = 30^\circ$.

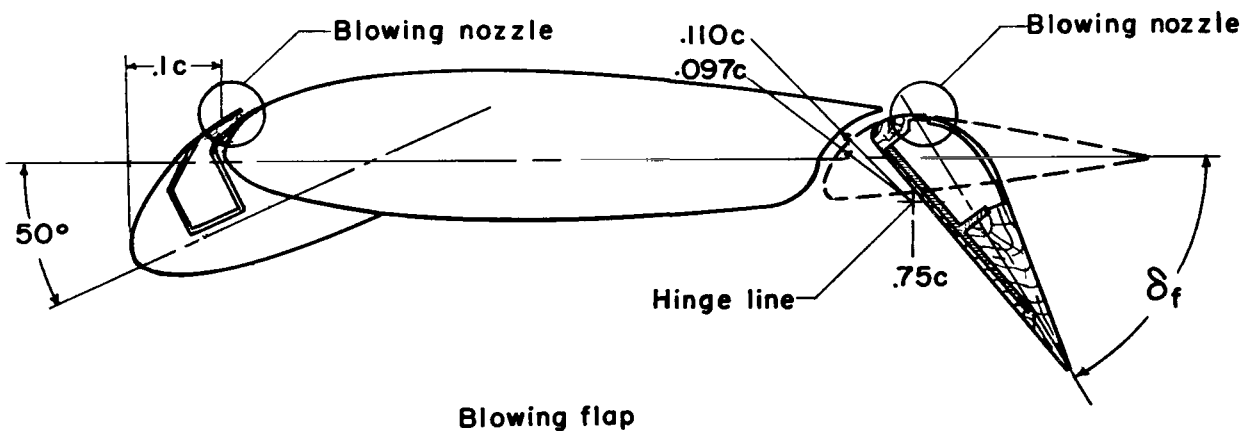
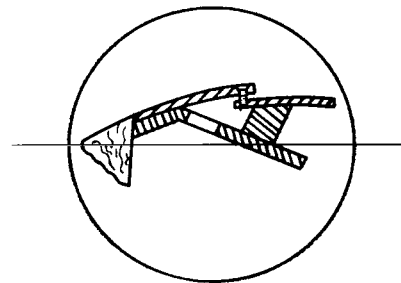
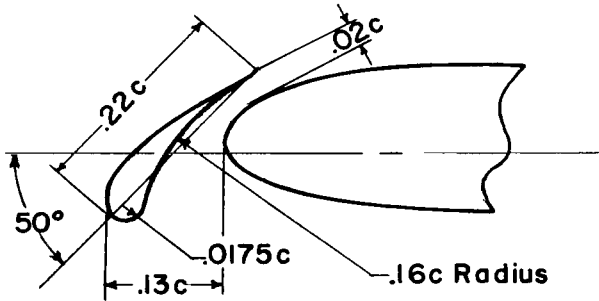
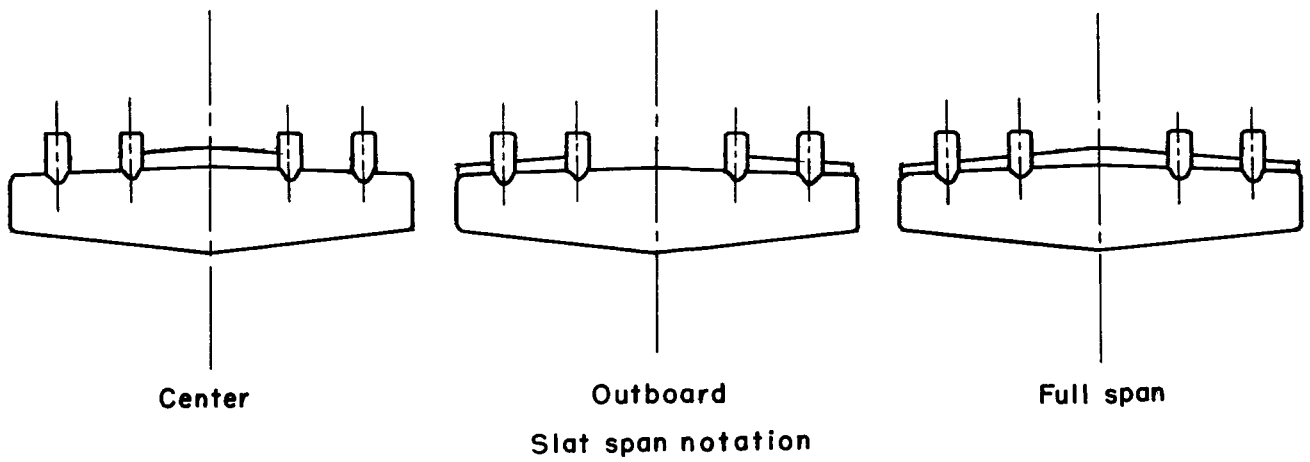


Dimensions in feet



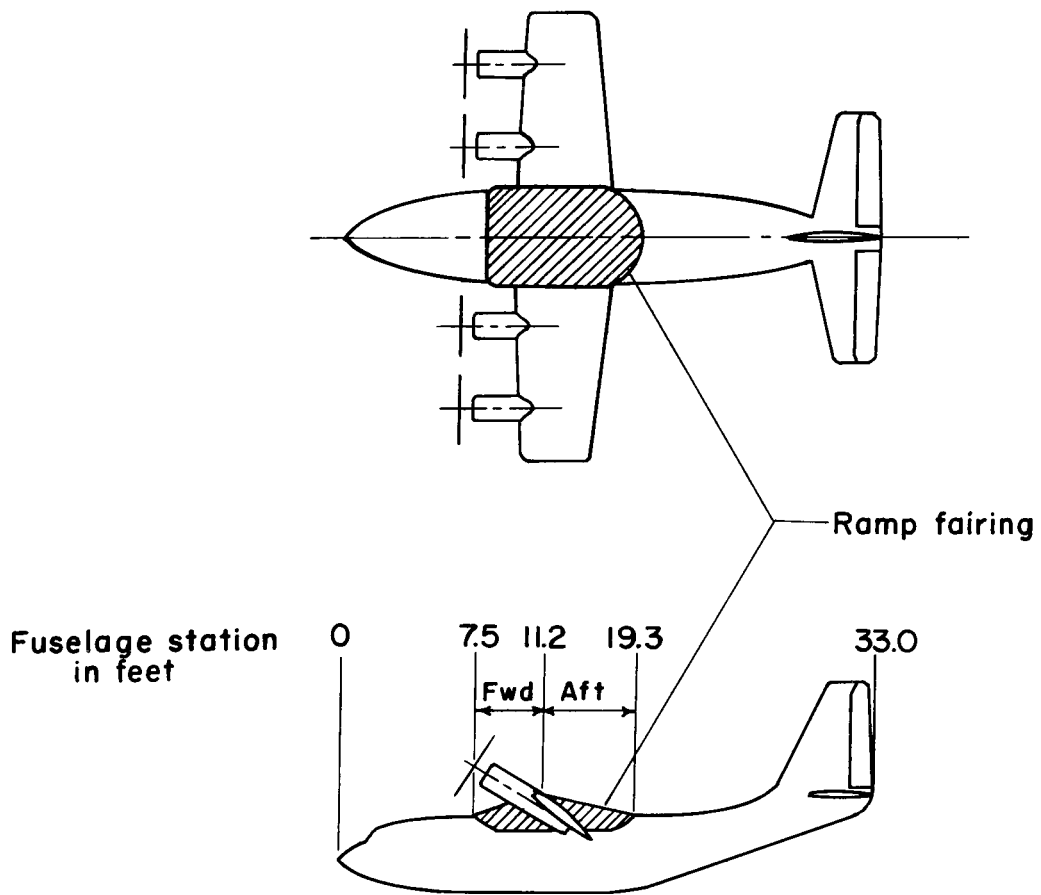
(a) General dimensions.

Figure 2.- Geometry of the model.



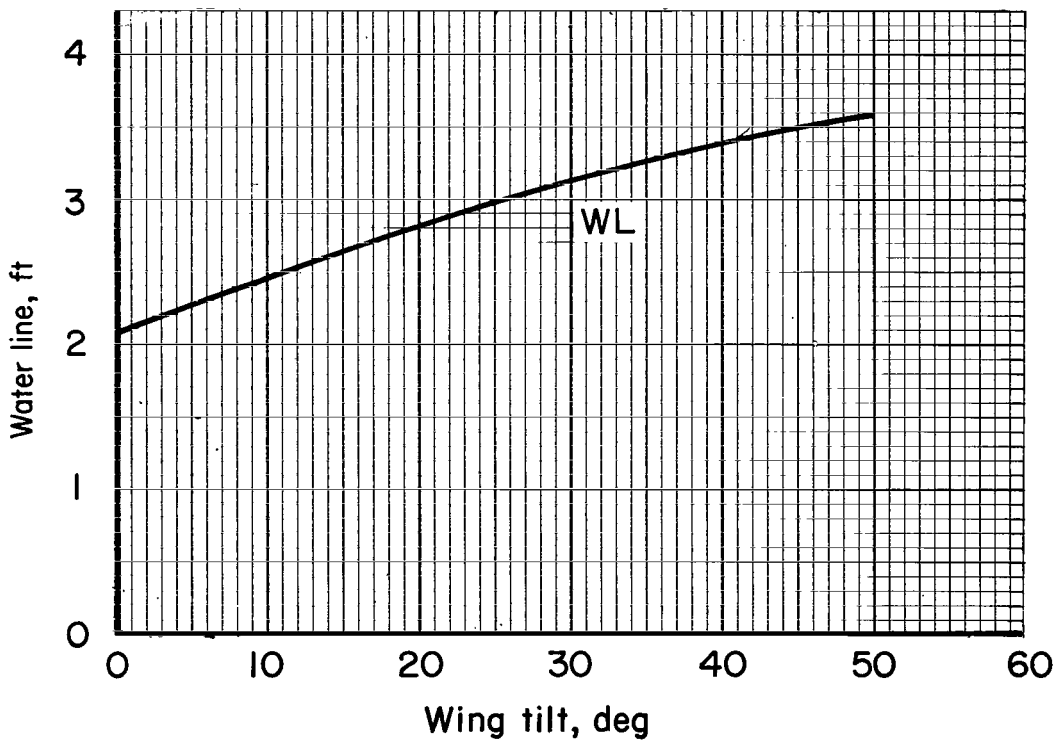
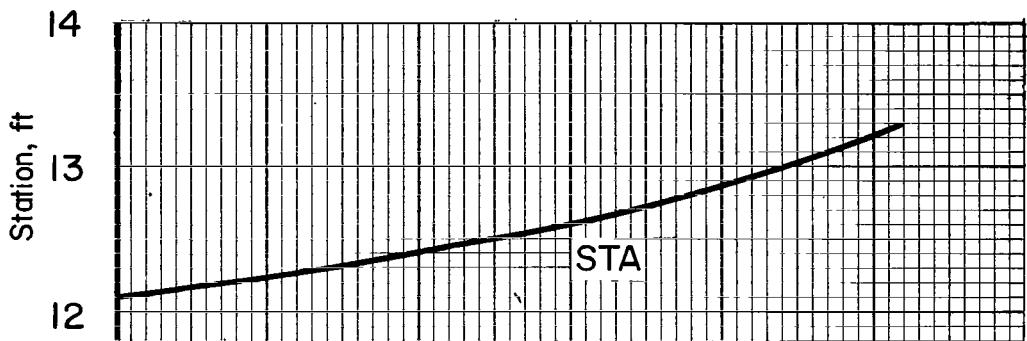
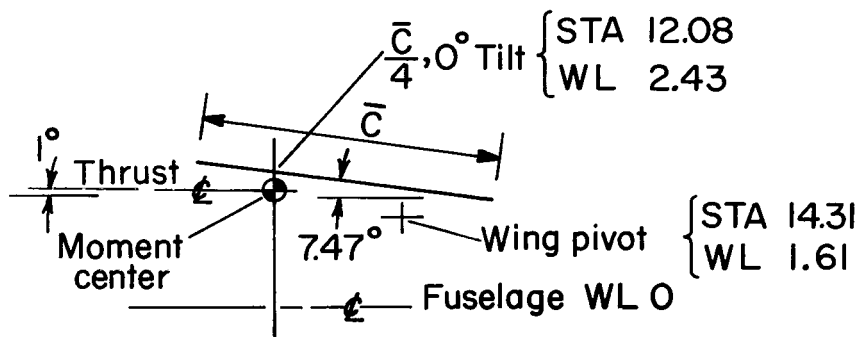
(b) Details of flaps and slats.

Figure 2.- Continued.



(c) Wing-fuselage ramp fairing.

Figure 2.- Continued.



(d) Moment center variation with wing tilt.

Figure 2.- Concluded.

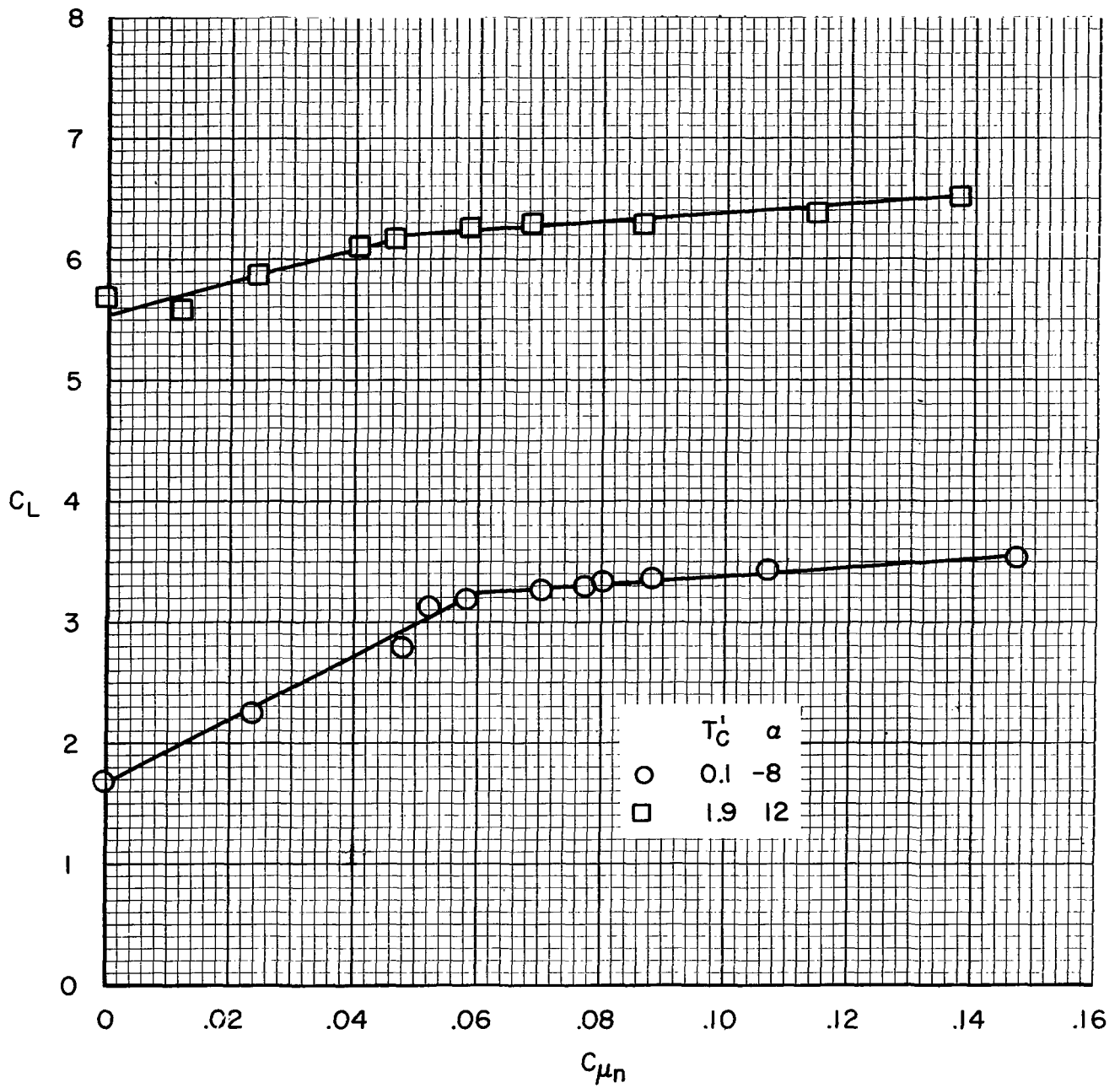


Figure 3.- Variation of lift coefficient with BLC nose flap momentum flow coefficient; $\delta_w = 30^\circ$, $\delta_f = 50^\circ$, $C_{\mu_f} = 0.065$.

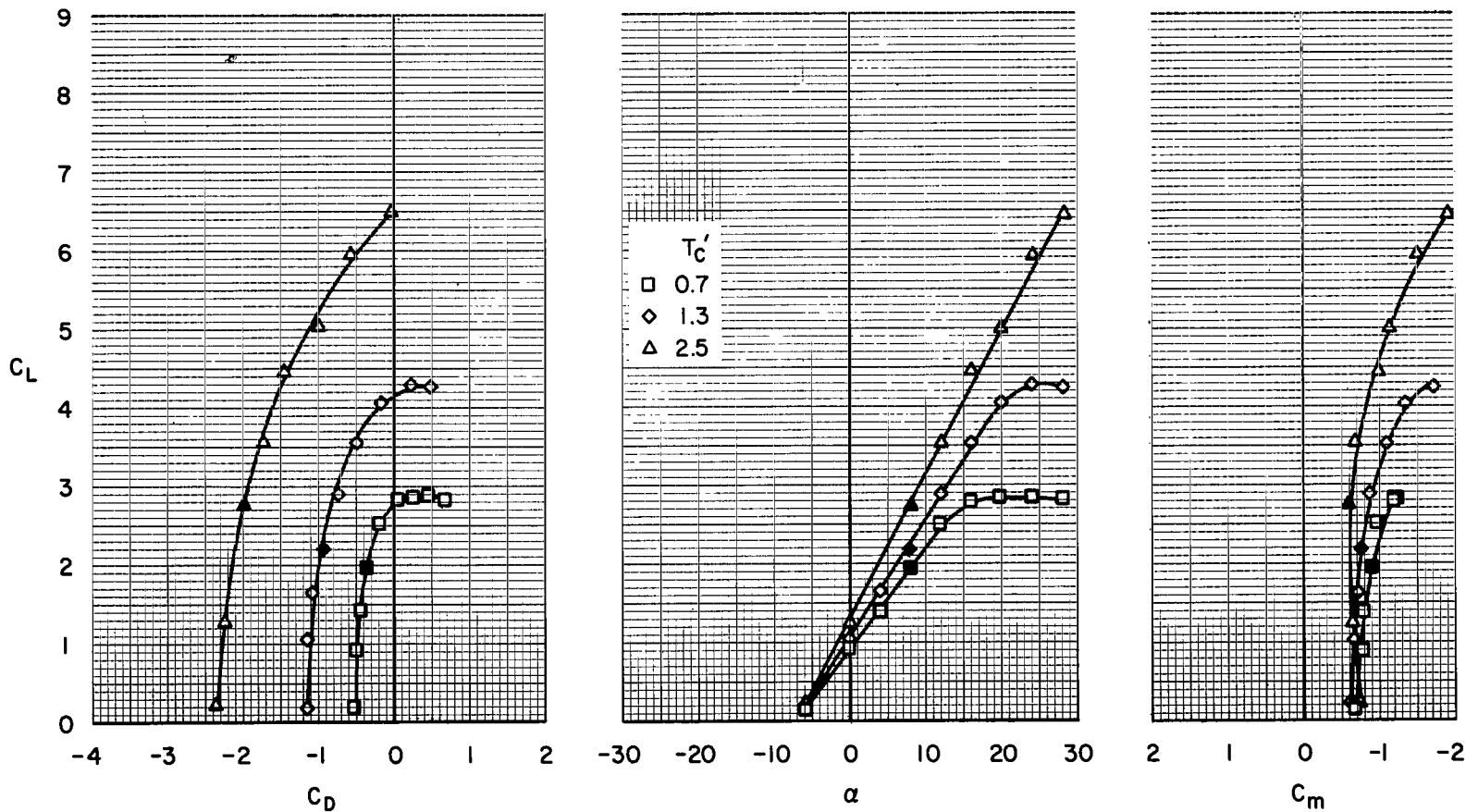
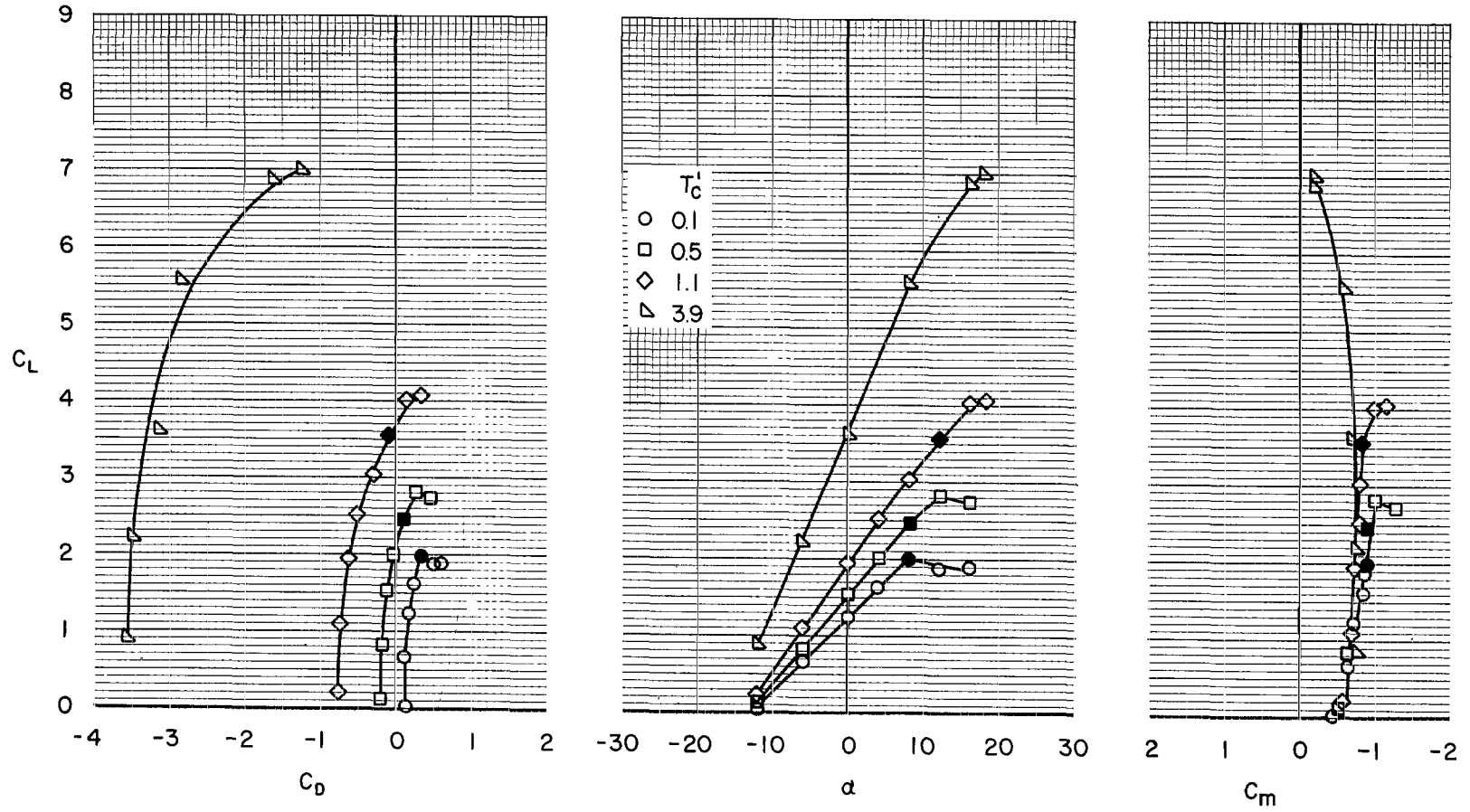
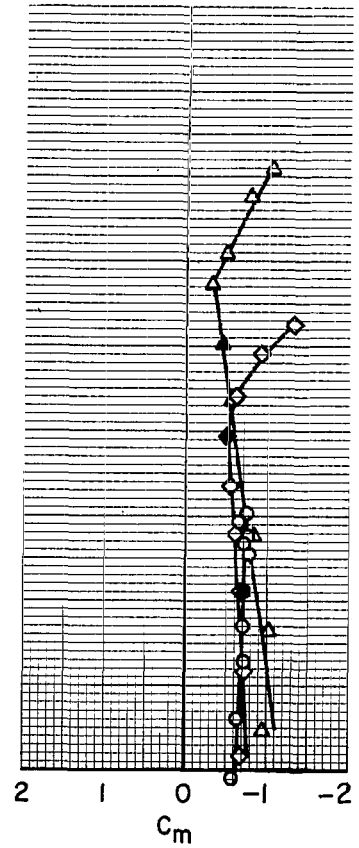
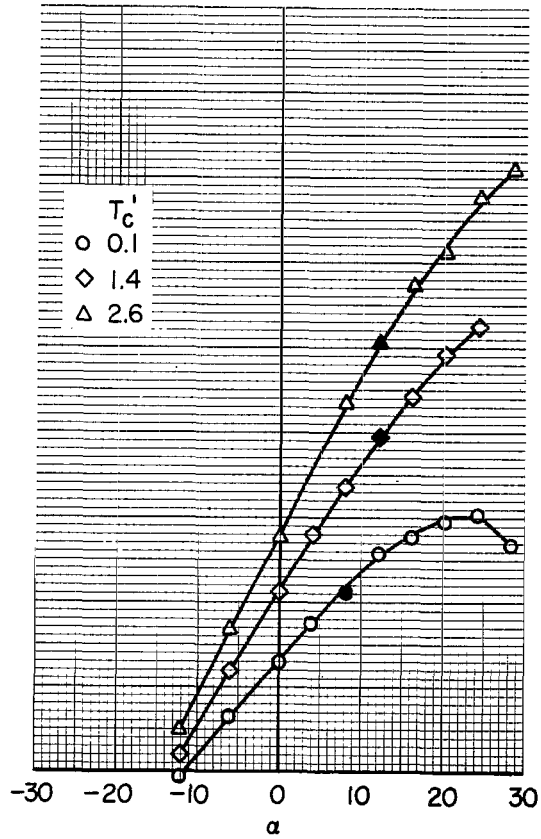
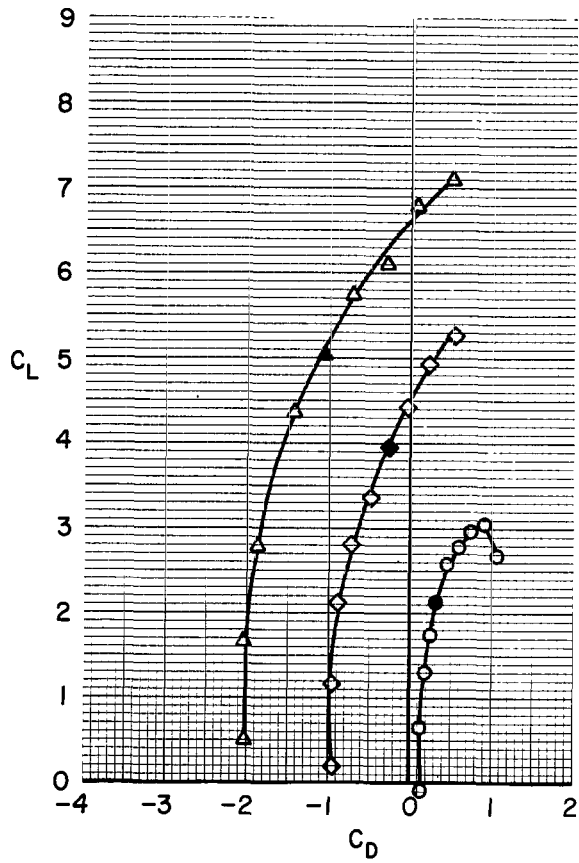


Figure 4.- Aerodynamic characteristics of the model; $\delta_w = 0^\circ$, $\delta_f = 0^\circ$, $i_t = 14^\circ$.



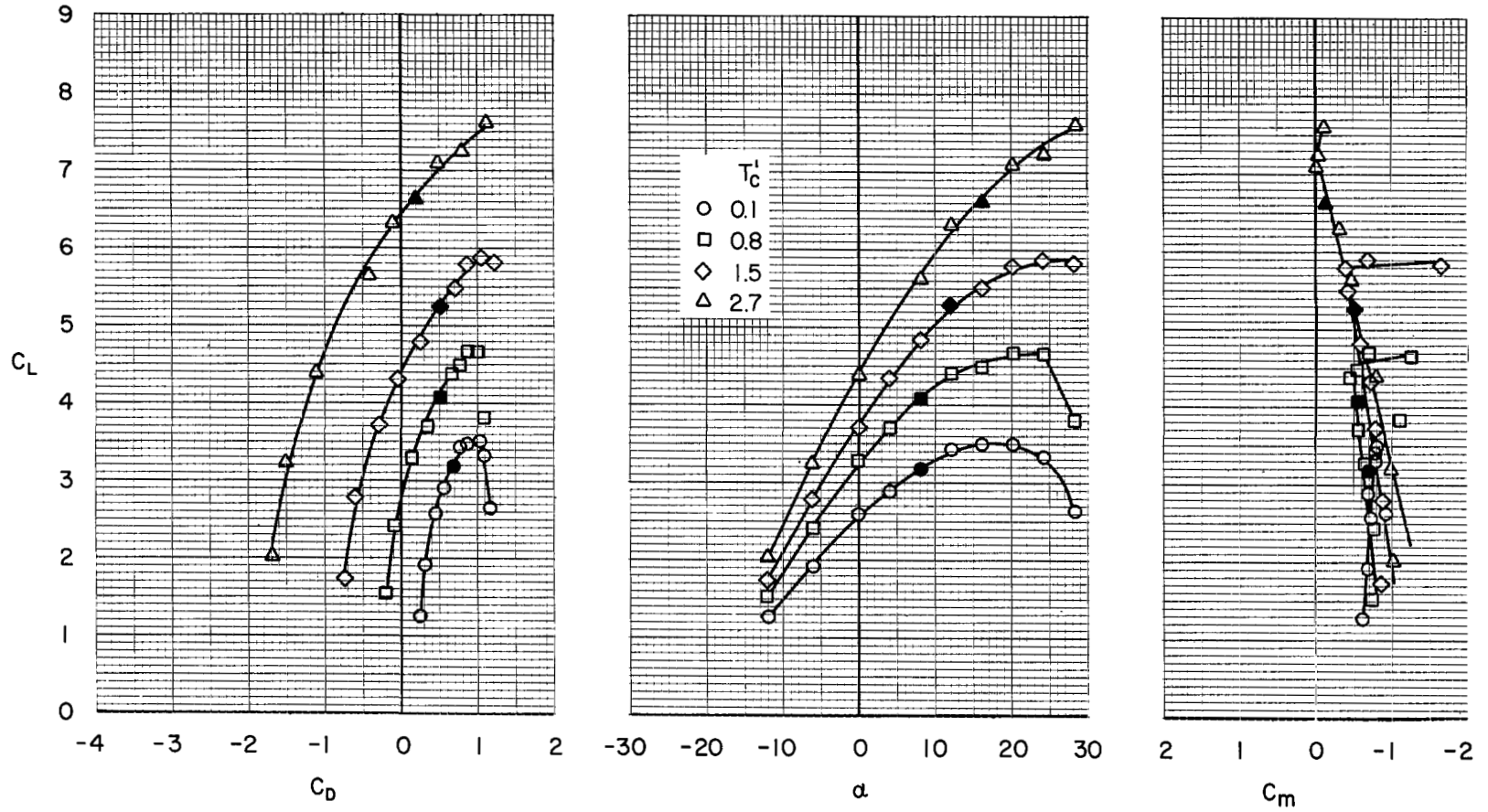
(a) $\delta_f = 30^\circ, C_{\mu_f} = 0$

Figure 5.- Aerodynamic characteristics of the model; $\delta_w = 0^\circ, i_t = 14^\circ$.



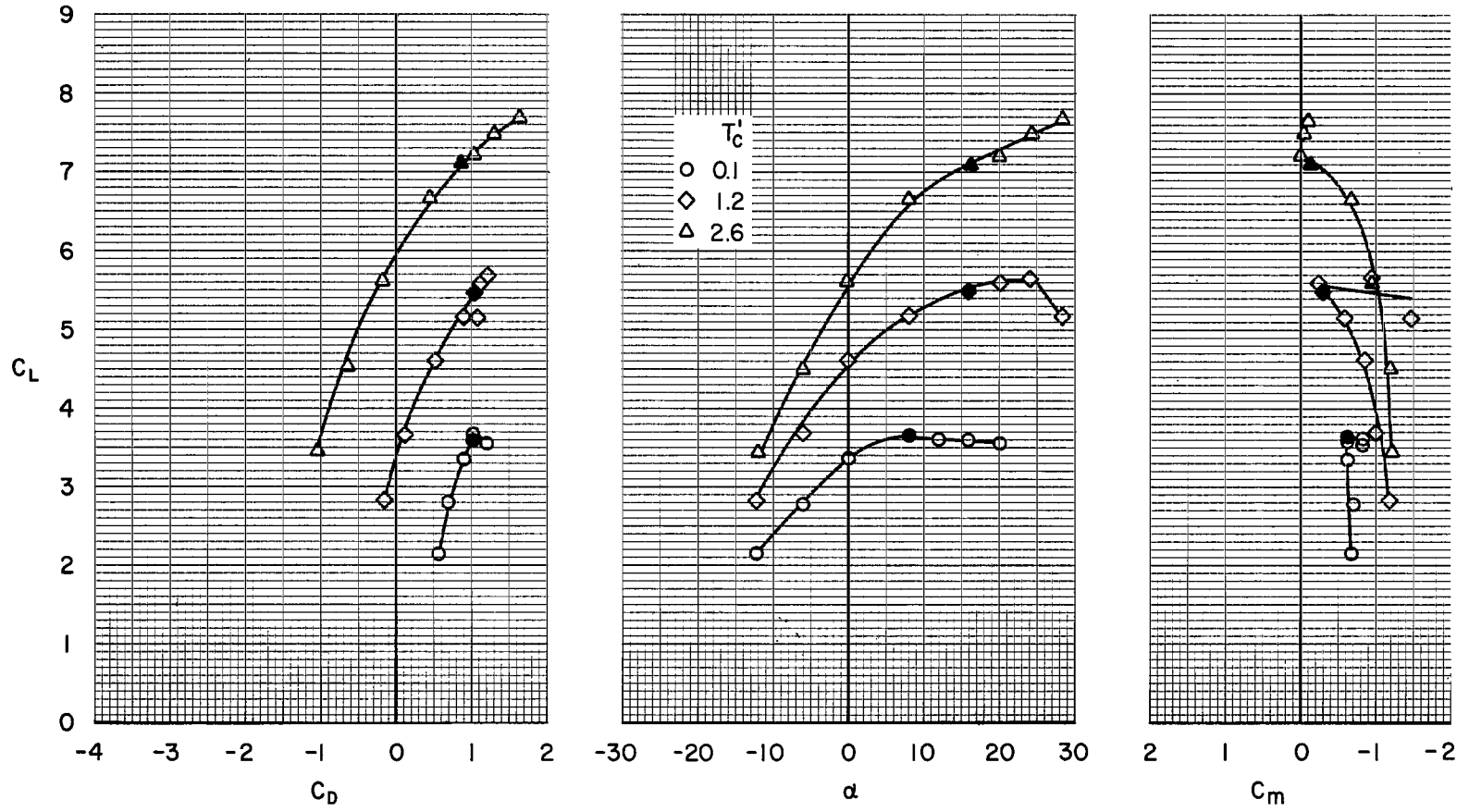
(b) $\delta_f = 30^\circ$, $C_{\mu_f} = 0$, full-span slat.

Figure 5.- Continued.



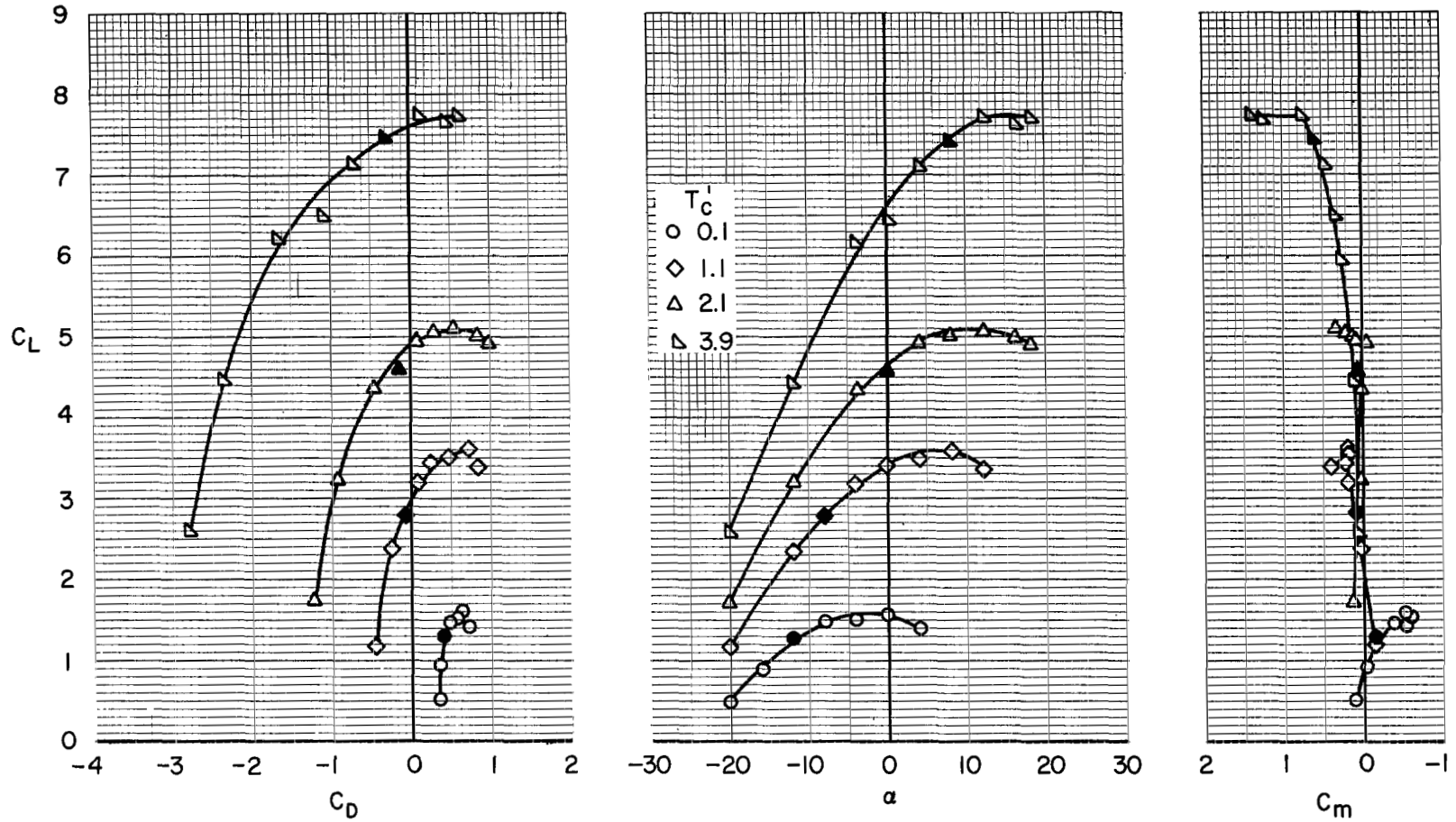
(c) $\delta_f = 50^\circ$, $C_{\mu_f} = 0.065$, full-span slat.

Figure 5.- Continued.



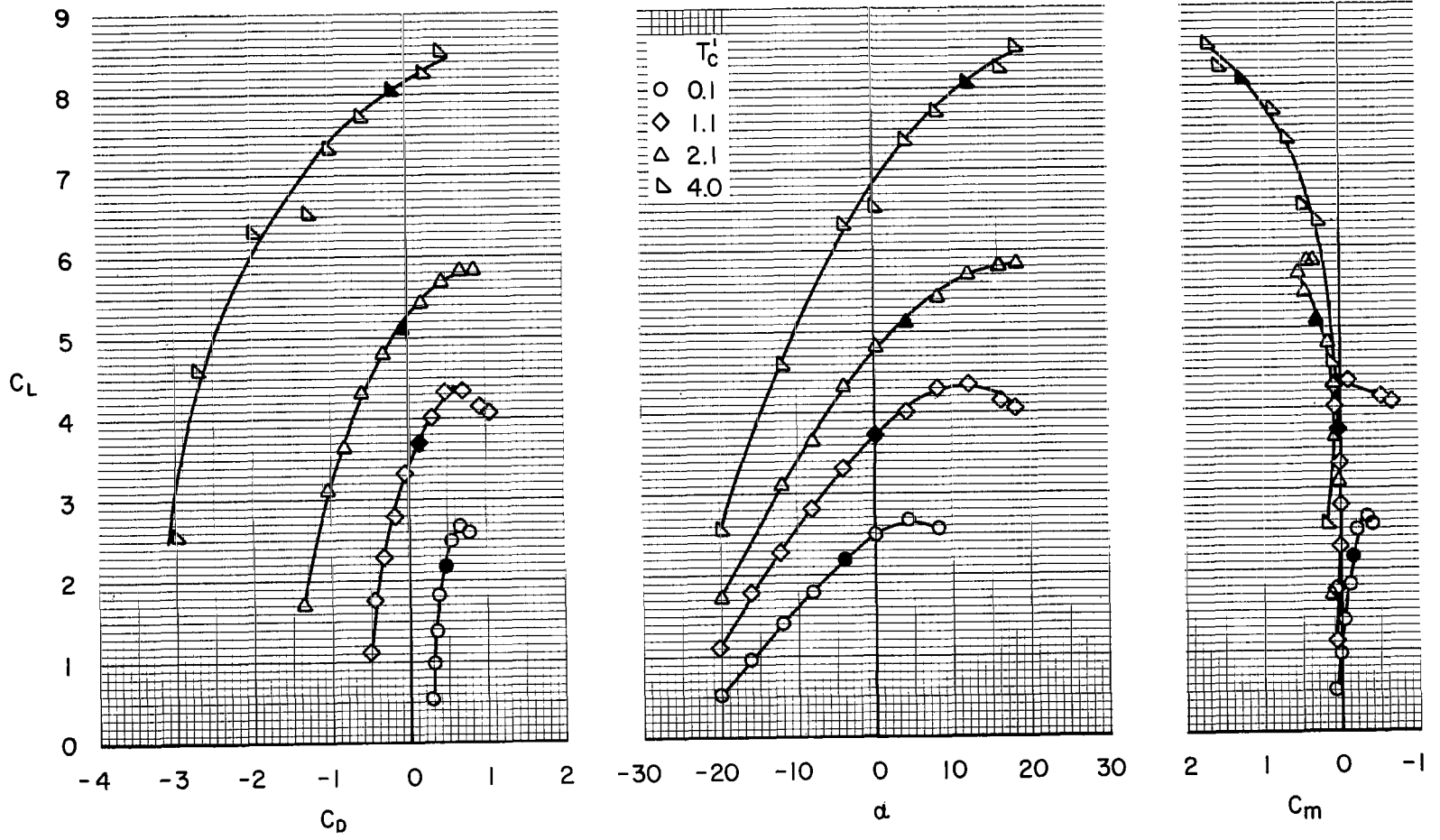
(d) $\delta_f = 80^\circ$, $C_{\mu_f} = 0.088$, full-span slat.

Figure 5.- Concluded.



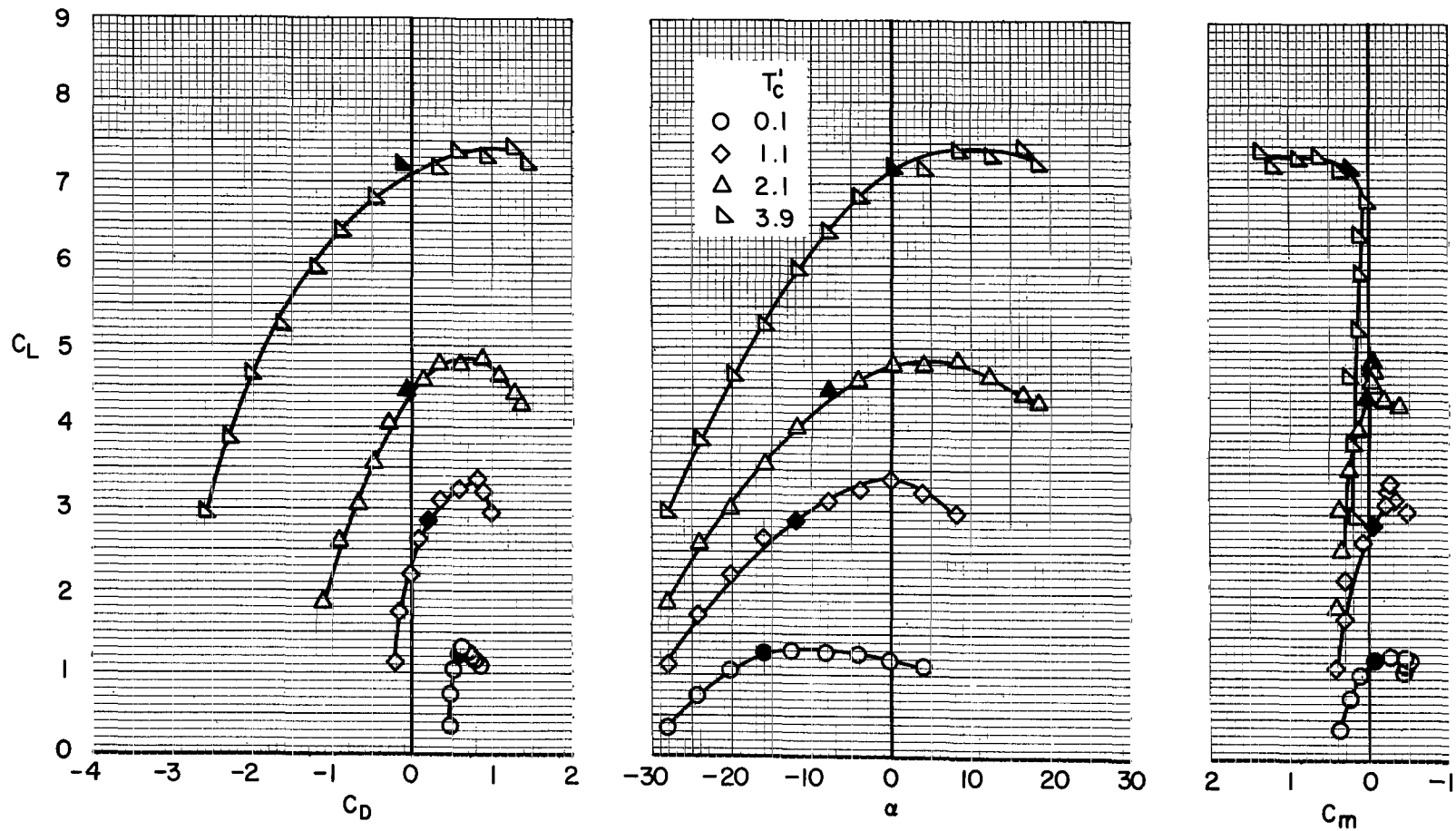
(a) $\delta_f = 30^\circ$, $C_{\mu_f} = 0$

Figure 6.- Aerodynamic characteristics of the model; $\delta_w = 20^\circ$, $i_t = 14^\circ$.



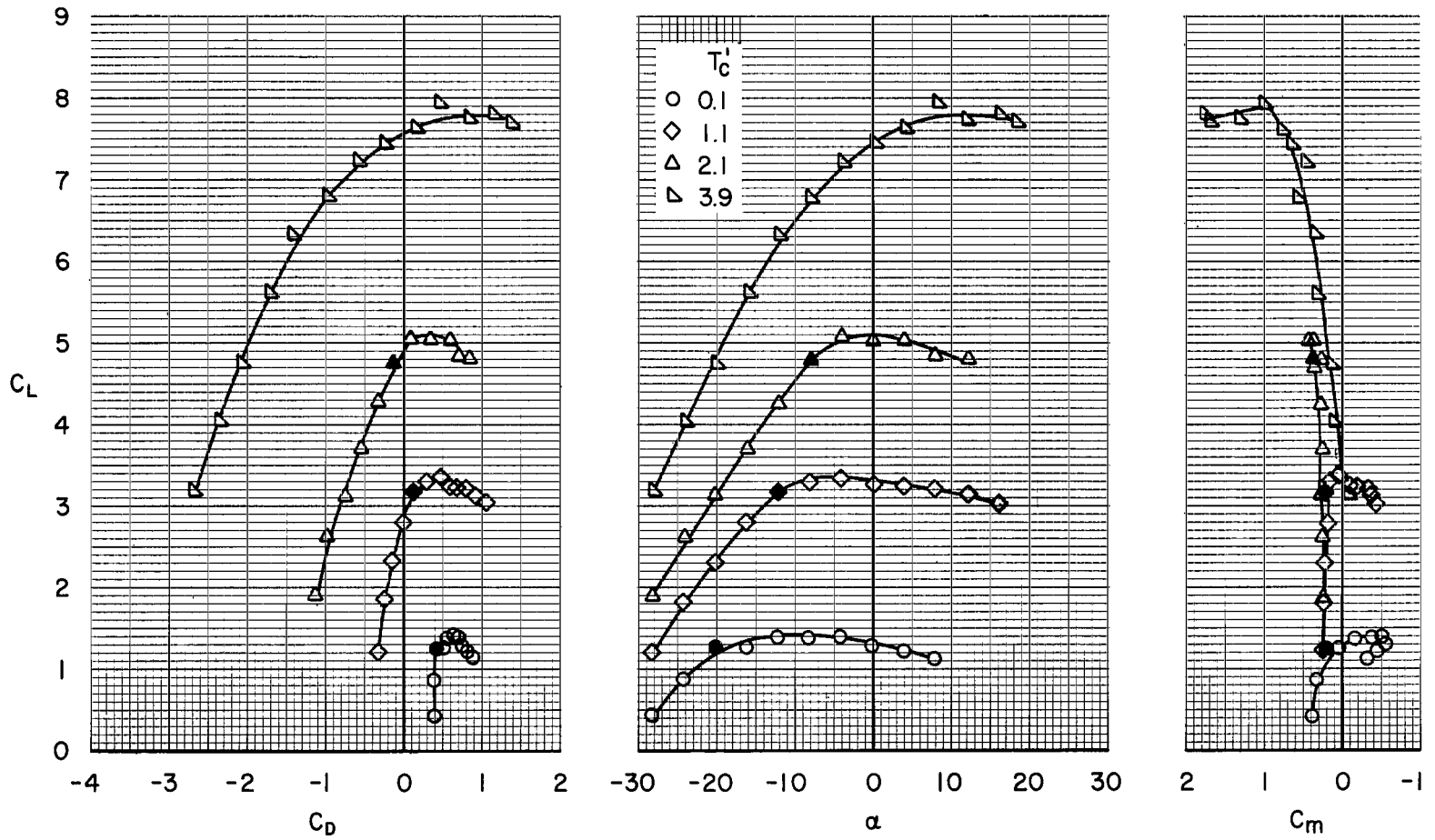
(b) $\delta_F = 30^\circ$, $C_{\mu_F} = 0$, full-span slat.

Figure 6.- Concluded.



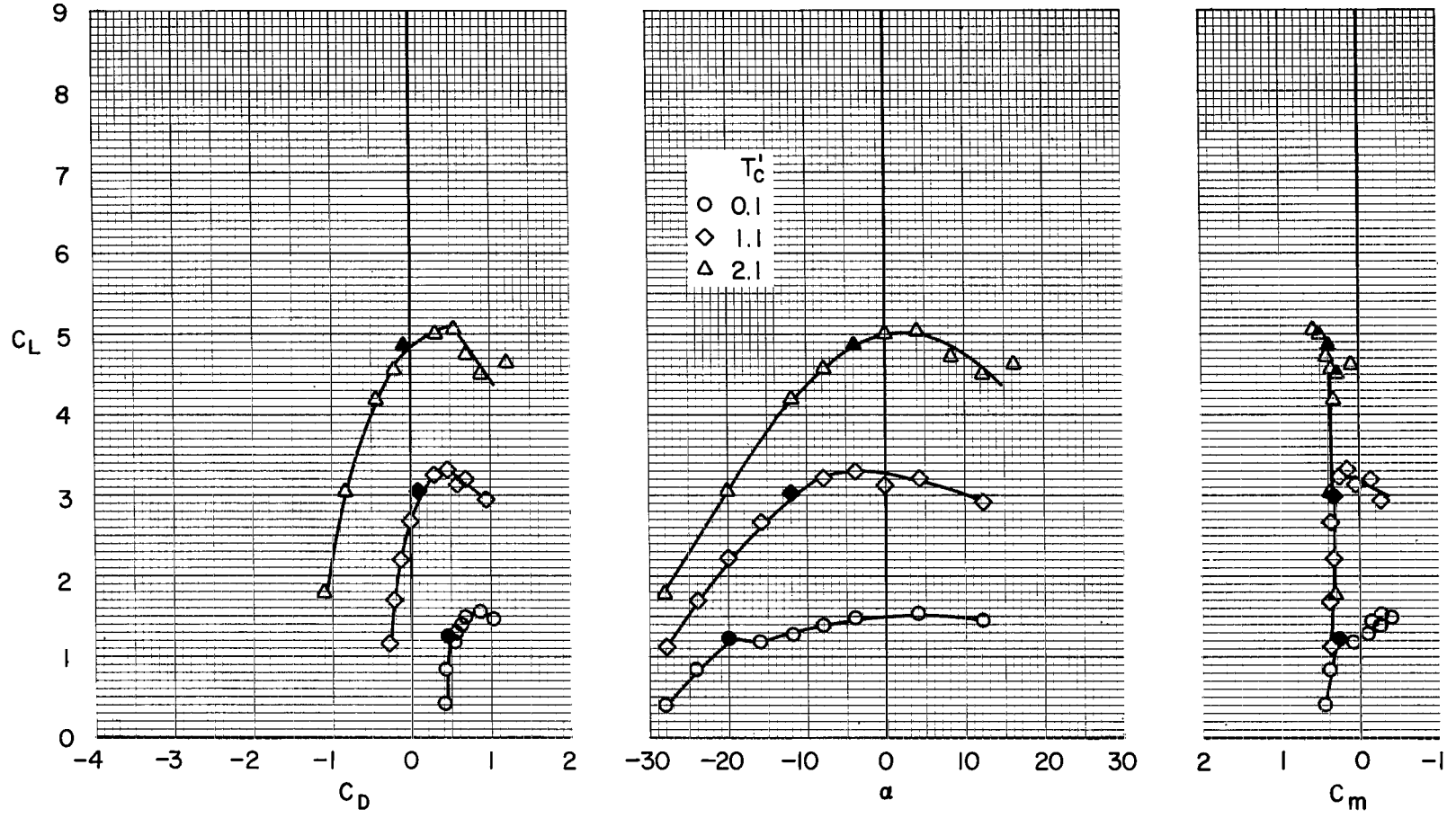
(a) $\delta_F = 30^\circ$, $C_{\mu_F} = 0$

Figure 7.- Aerodynamic characteristics of the model; $\delta_w = 30^\circ$, $i_t = 14^\circ$.



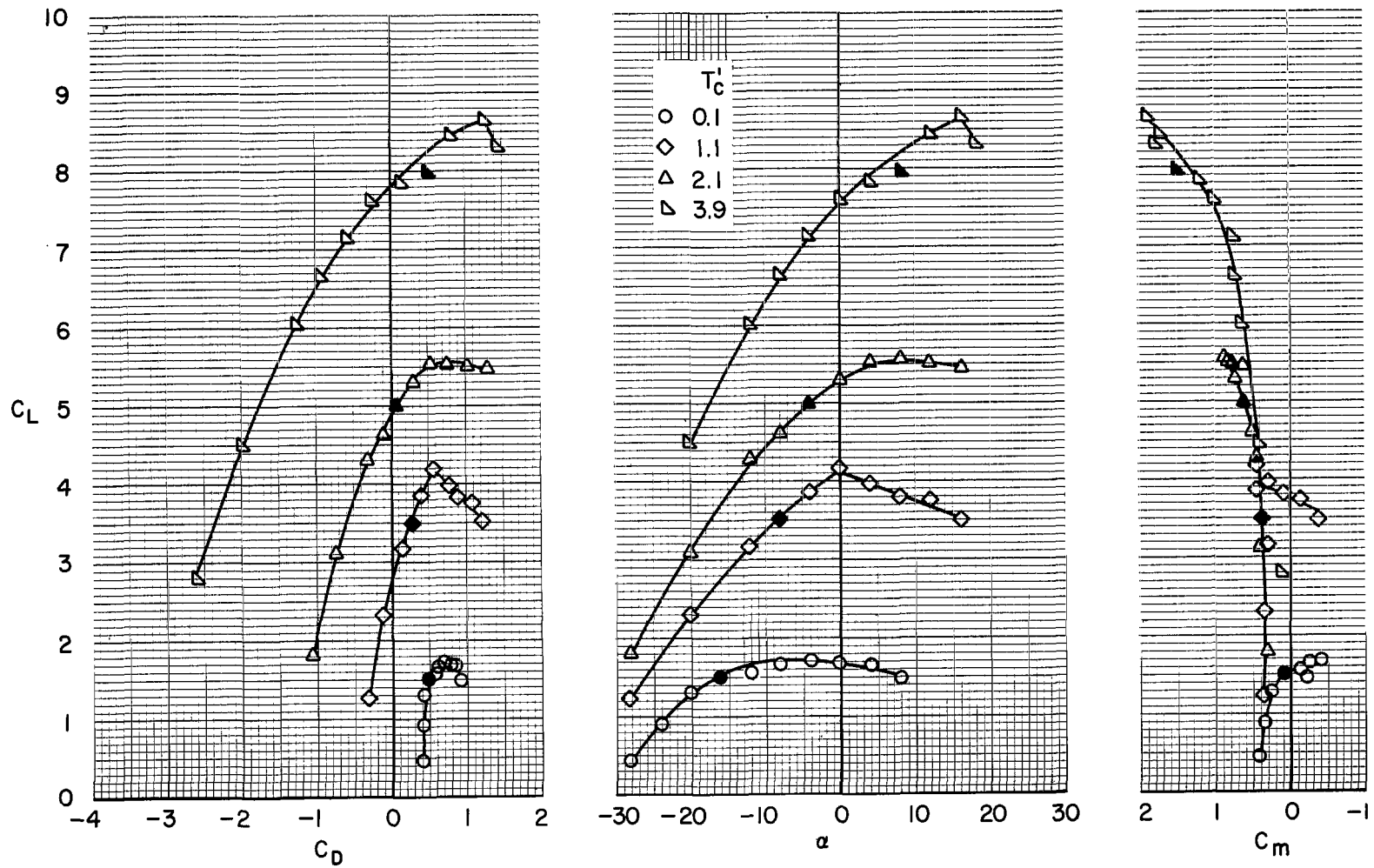
(b) $\delta_f = 30^\circ$, $C_{\mu_f} = 0$, ramp.

Figure 7.- Continued.



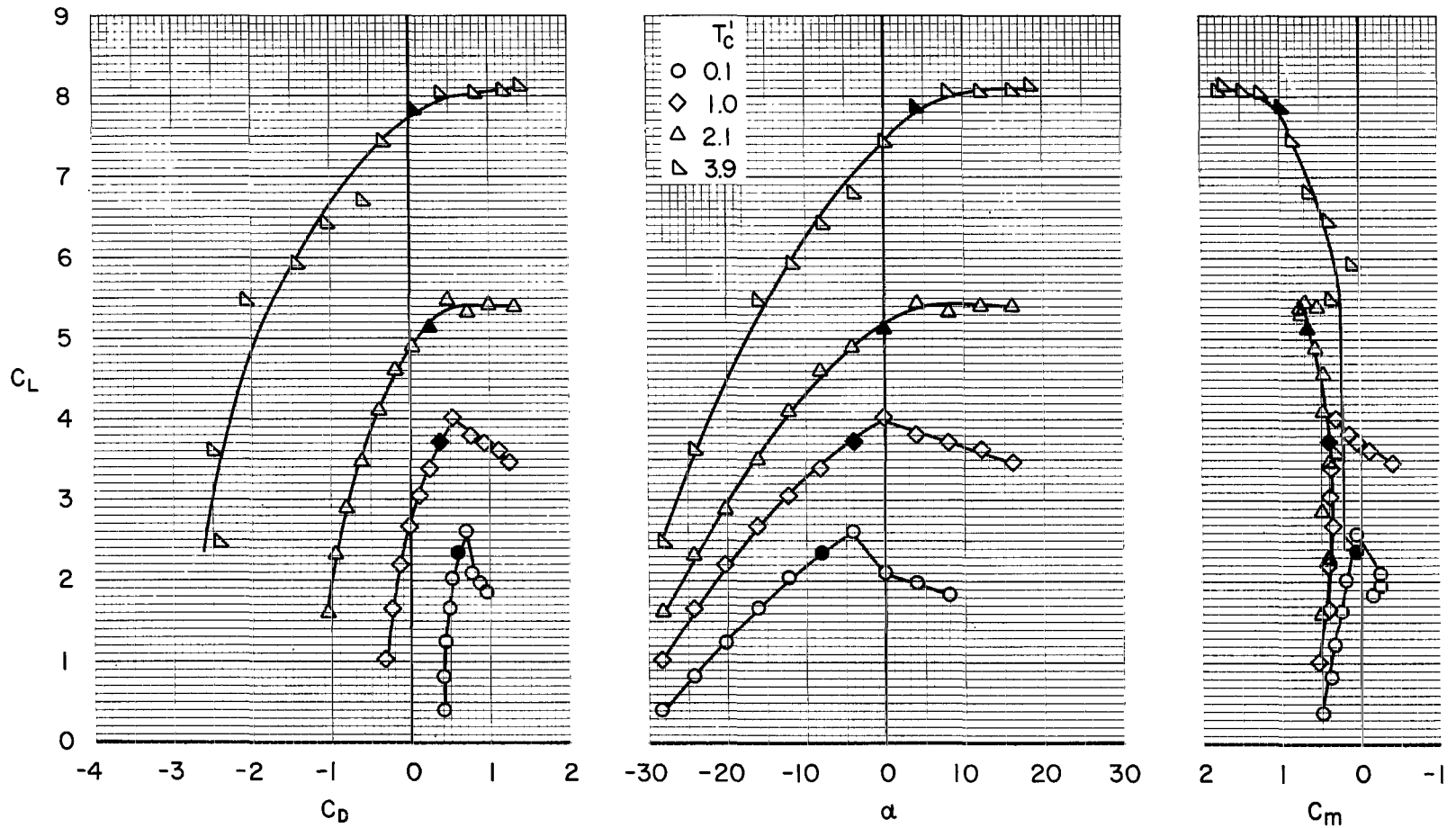
(c) $\delta_f = 30^\circ$, $C_{\mu_f} = 0$, center slat.

Figure 7.- Continued.



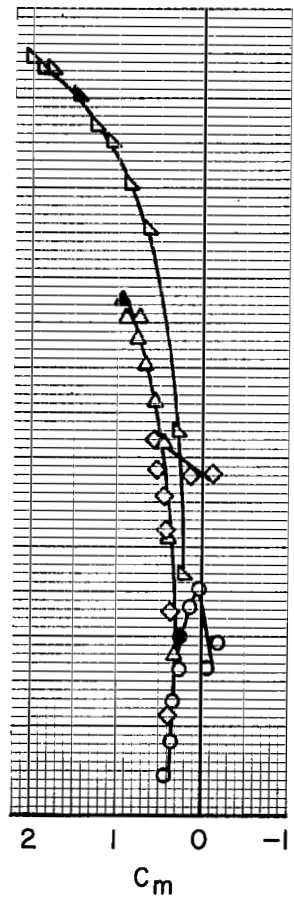
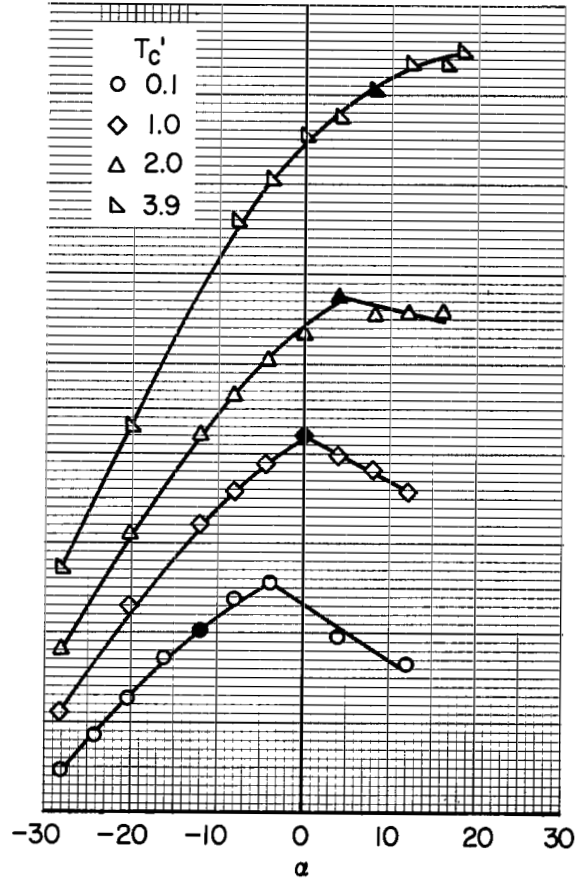
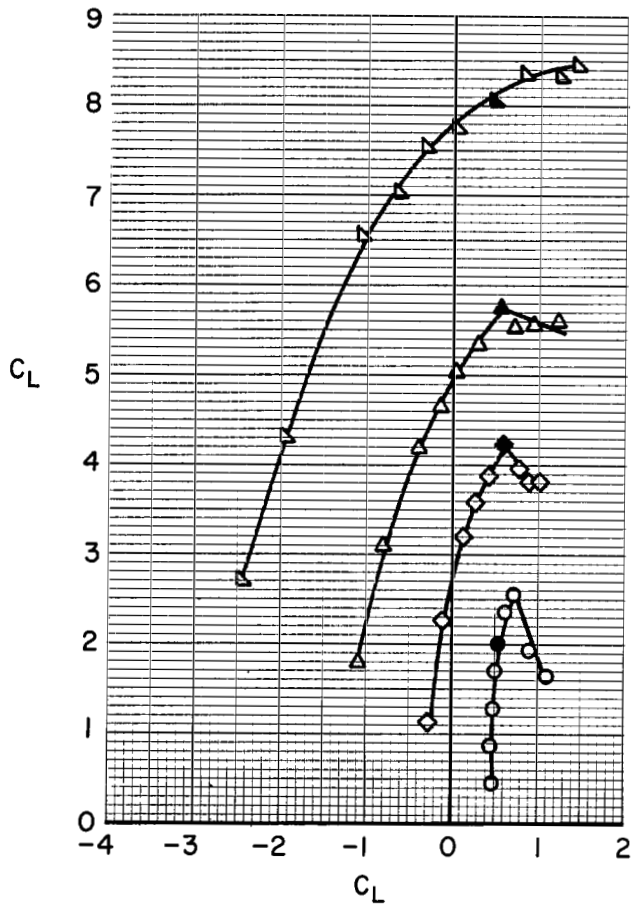
(d) $\delta_f = 30^\circ$, $C_{\mu_f} = 0$, ramp and outboard slat.

Figure 7.- Continued.



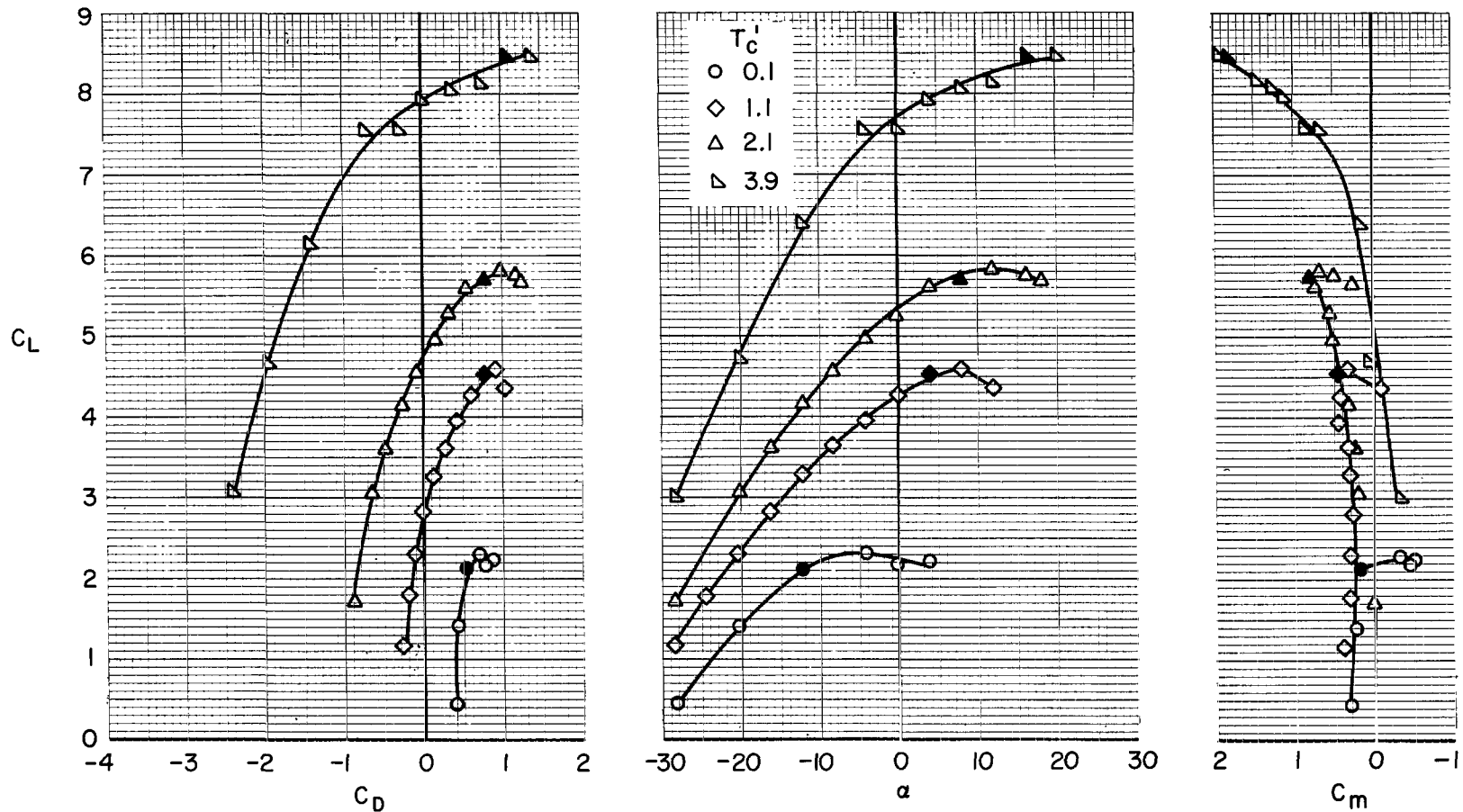
(e) $\delta_f = 30^\circ$, $C_{\mu_f} = 0$, full-span slat.

Figure 7.- Continued.



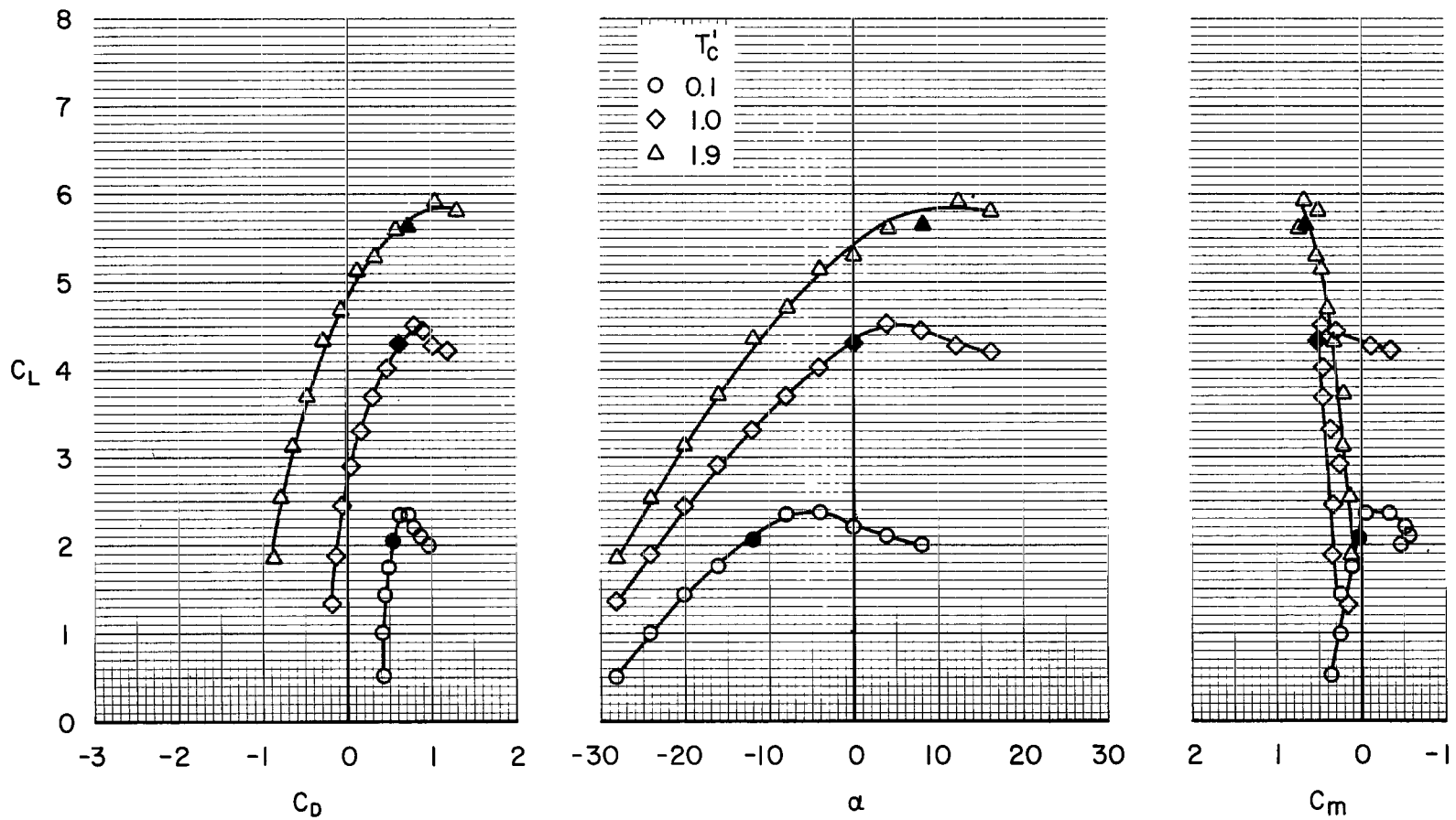
(f) $\delta_f = 30^\circ$, $C_{\mu_f} = 0$, ramp and full-span slat.

Figure 7.- Continued.



(g) $\delta_f = 30^\circ$, $C_{\mu_f} = 0$, ramp and BLC nose flap, $C_{\mu_n} = 0.070$.

Figure 7.- Continued.



(h) $\delta_F = 30^\circ$, $C_{\mu_F} = 0$, aft ramp and BLC nose flap, $C_{\mu_n} = 0.070$.

Figure 7.- Concluded.

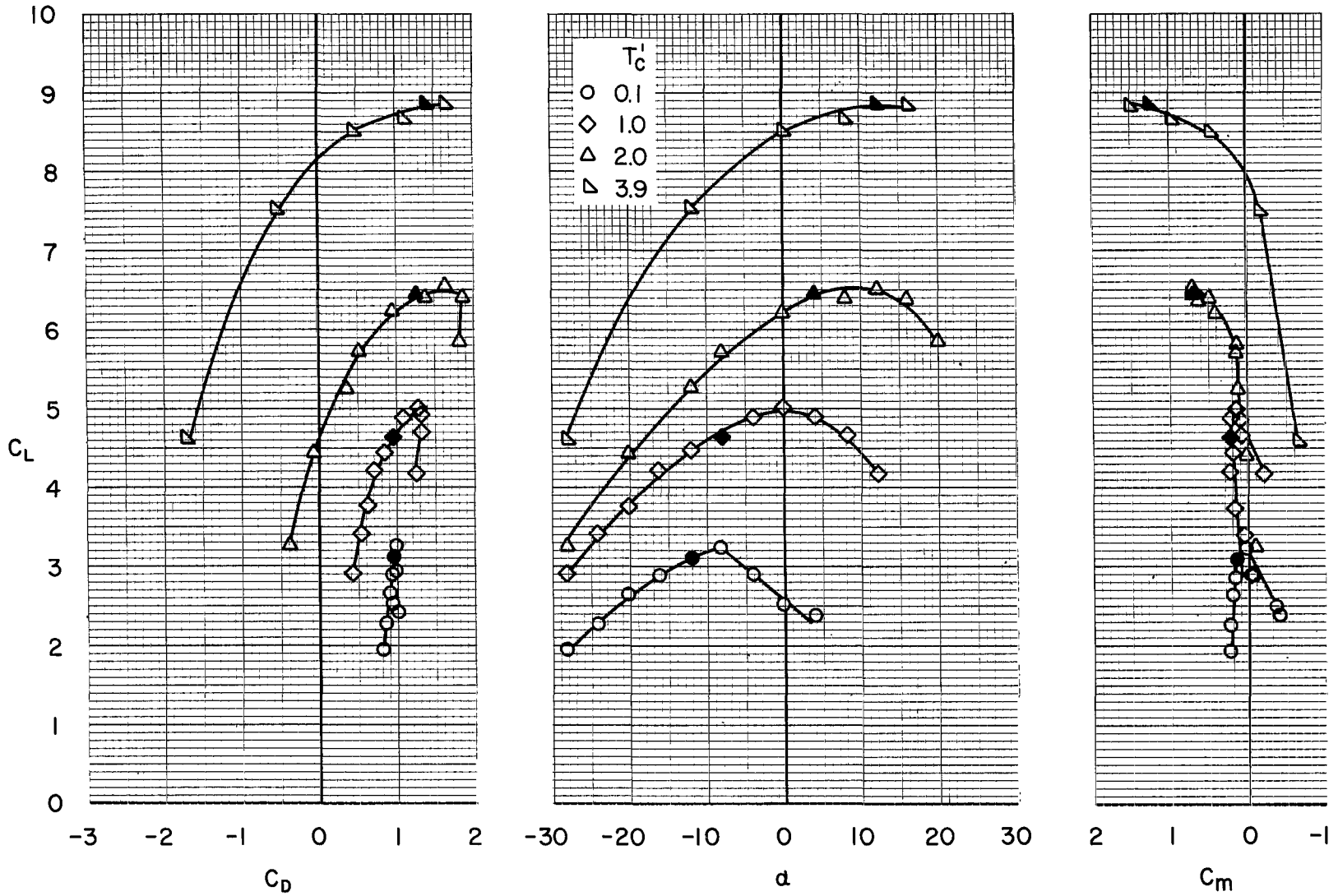


Figure 8.- Aerodynamic characteristics of the model; $\delta_w = 30^\circ$, $\delta_f = 50^\circ$, $C_{\mu_f} = 0.065$, BLC nose flap, $C_{\mu_n} = 0.074$, $i_t = 14^\circ$.

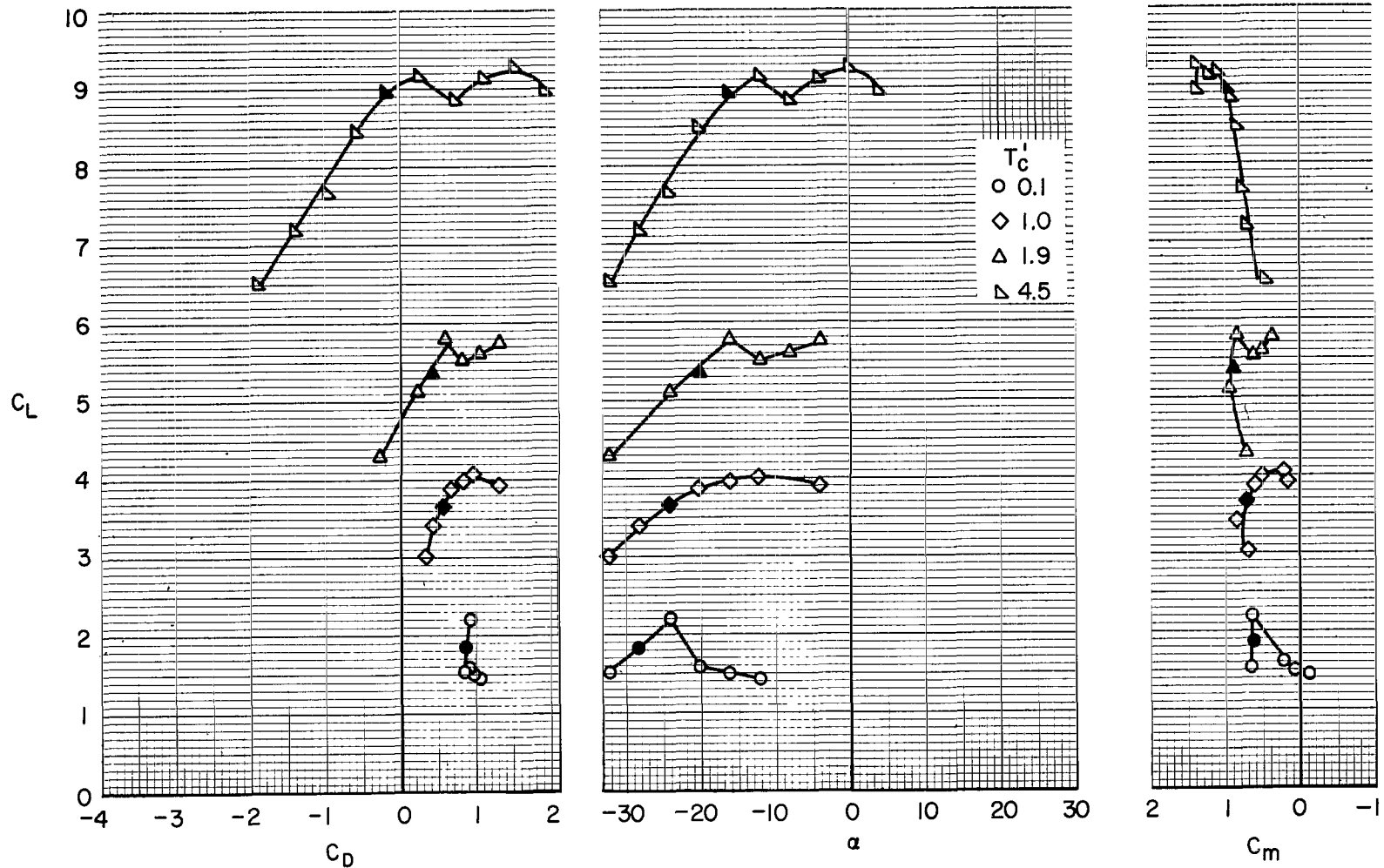
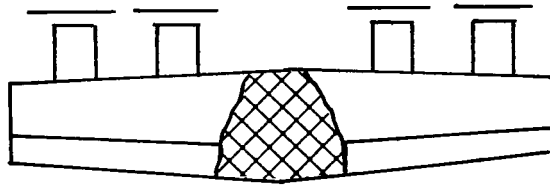


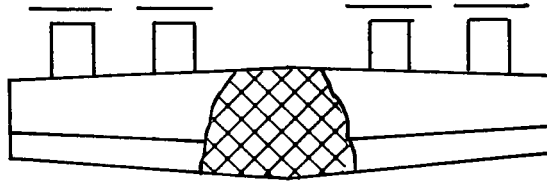
Figure 9.- Aerodynamic characteristics of the model; $\delta_w = 50^\circ$, $\delta_f = 30^\circ$, $C_{\mu_f} = 0$, full-span slat, $i_t = 14^\circ$.

 Rough flow

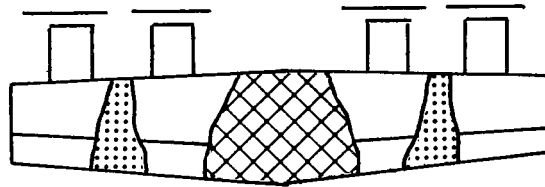
 Stalled



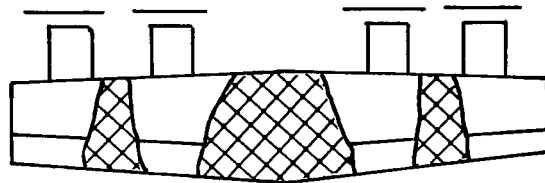
$\alpha = -16^\circ$



$\alpha = -12^\circ$



$\alpha = -8^\circ$



$\alpha = -4^\circ$

Figure 10.- Wing flow separation patterns; $\delta_w = 30^\circ$, $\delta_f = 30^\circ$, $C_{\mu_f} = 0$, $T_c' = 1.1$ (force data in fig. 7(a)).

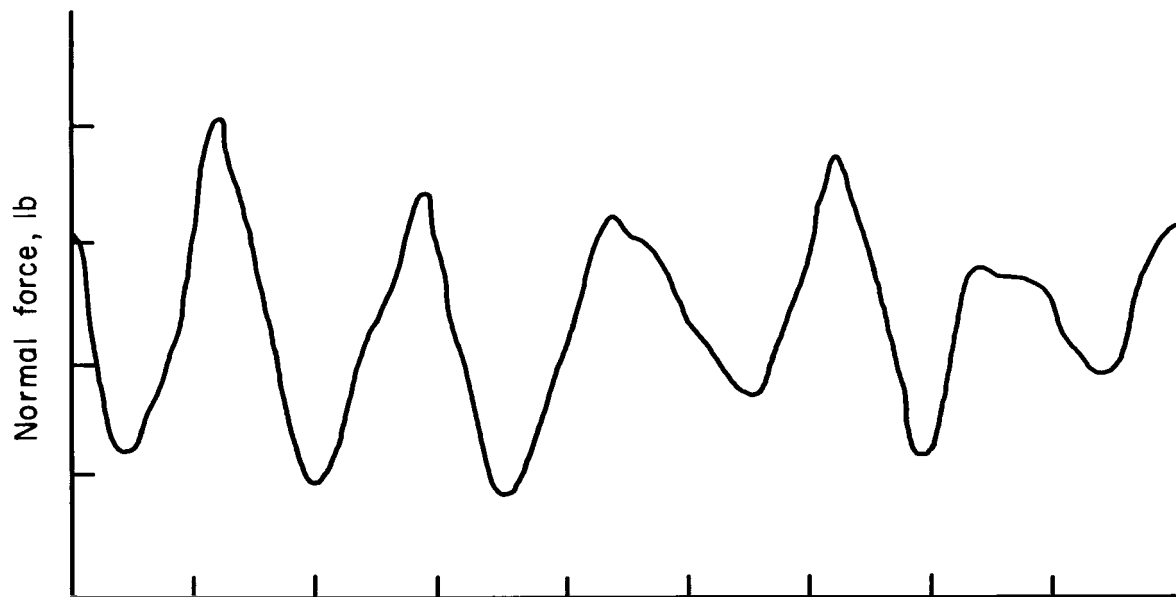
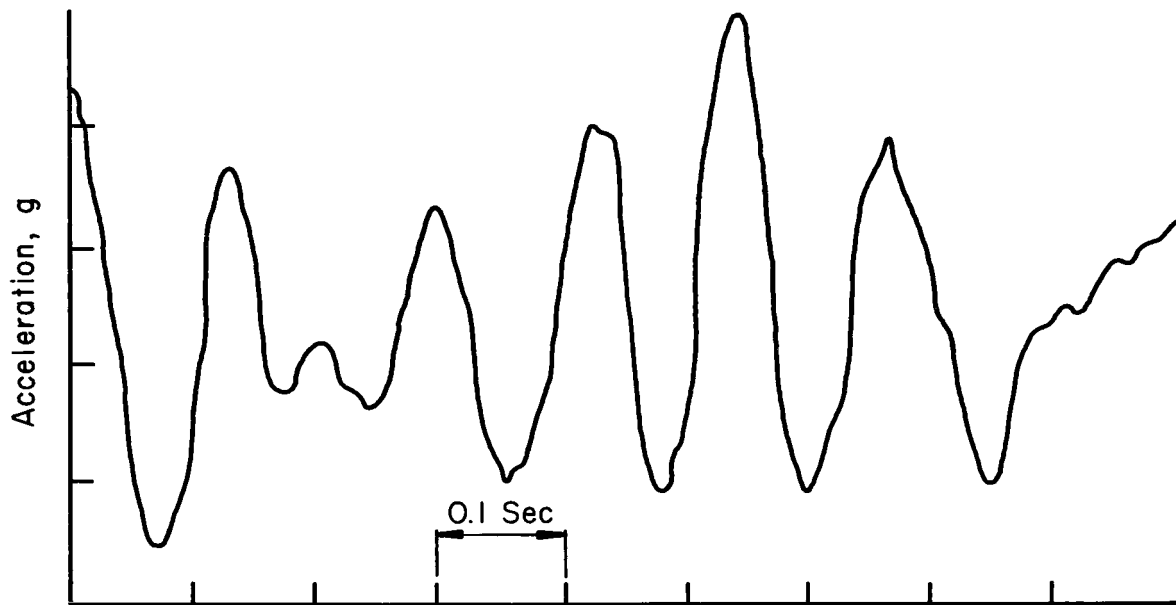


Figure 11.- Examples of oscillograph records of buffet loads on the model.

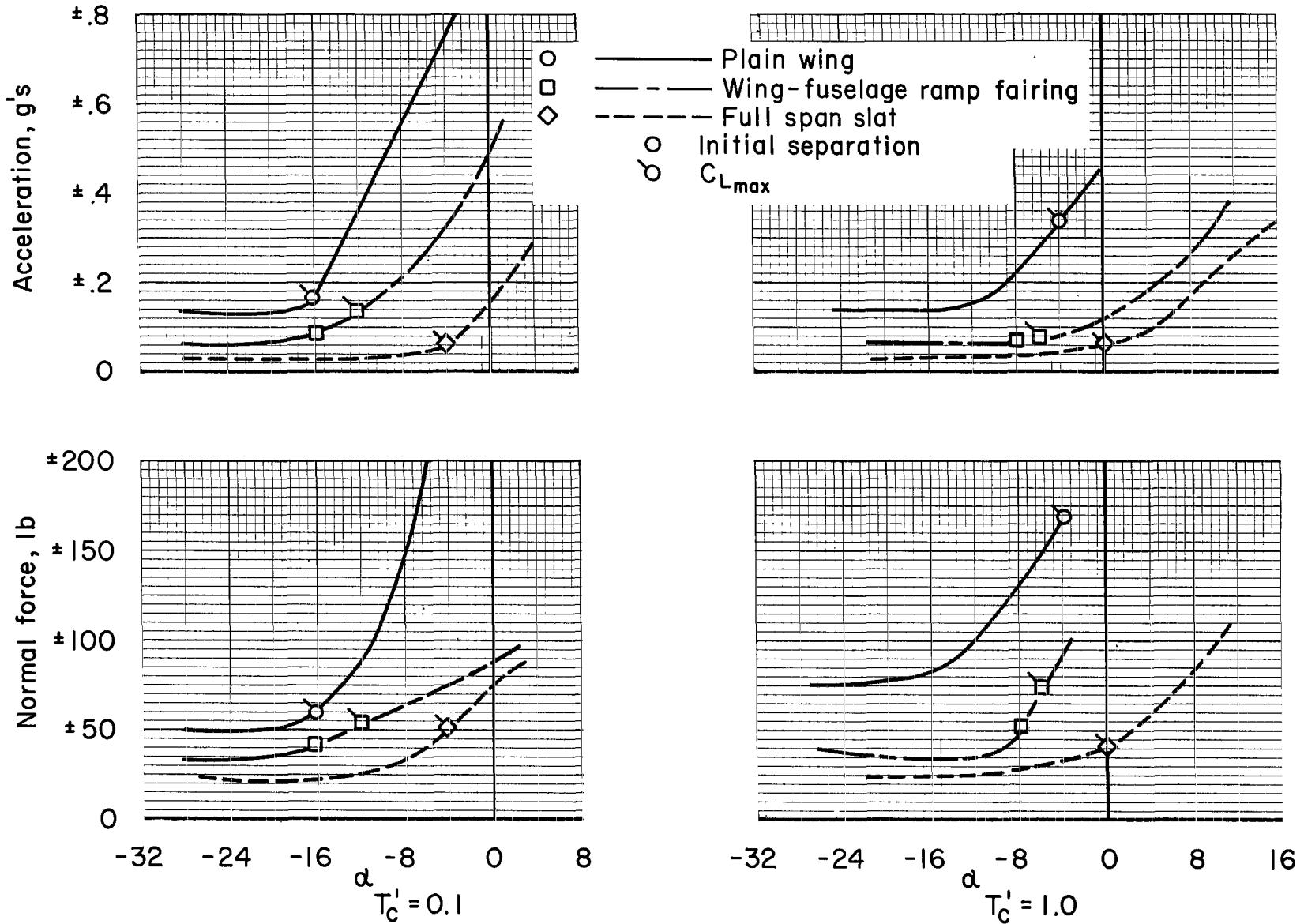


Figure 12.- Variation of fluctuating loads with angle of attack; $\delta_w = 30^\circ$, $\delta_f = 30^\circ$, $C_{\mu_f} = 0$.

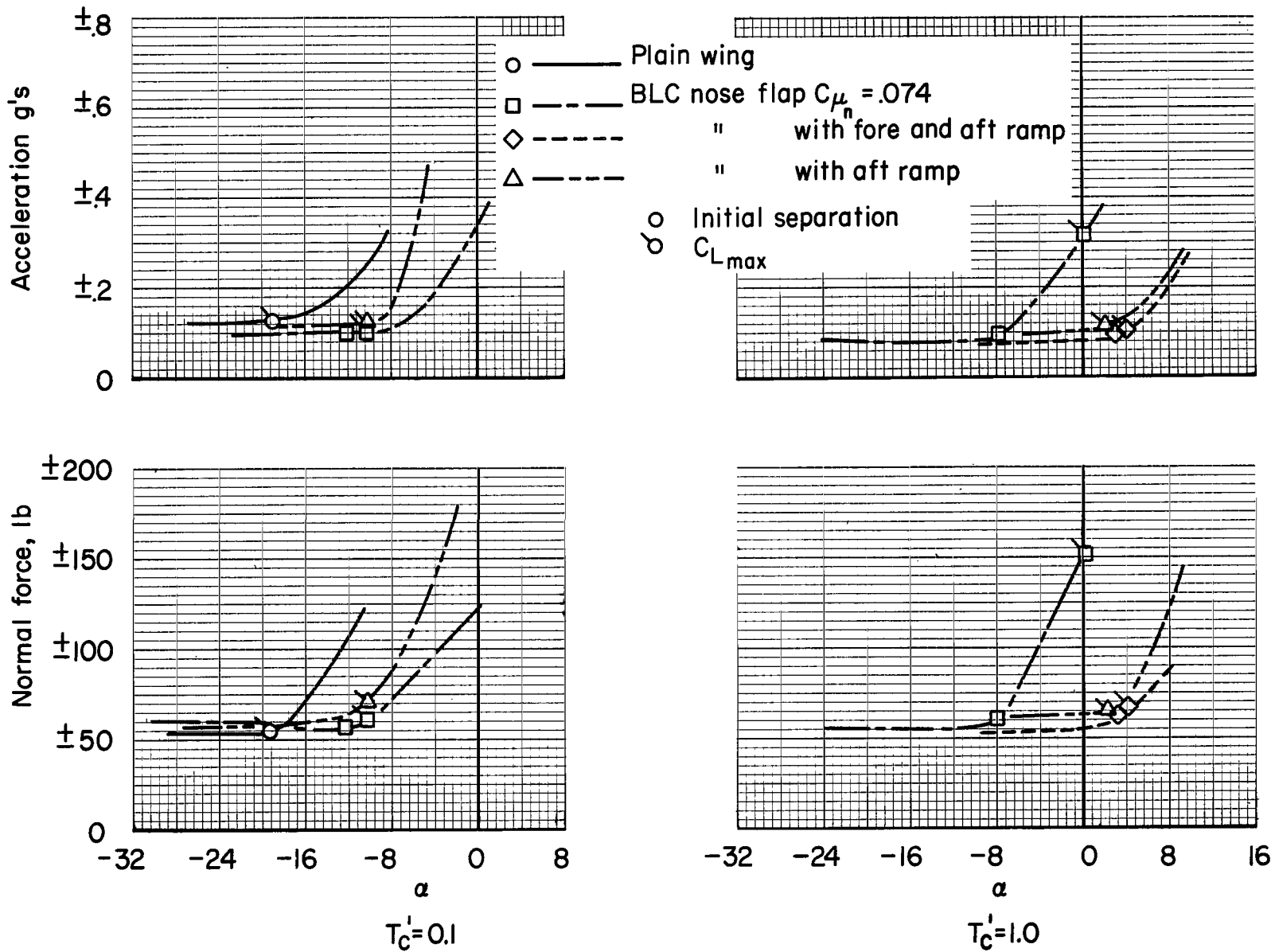
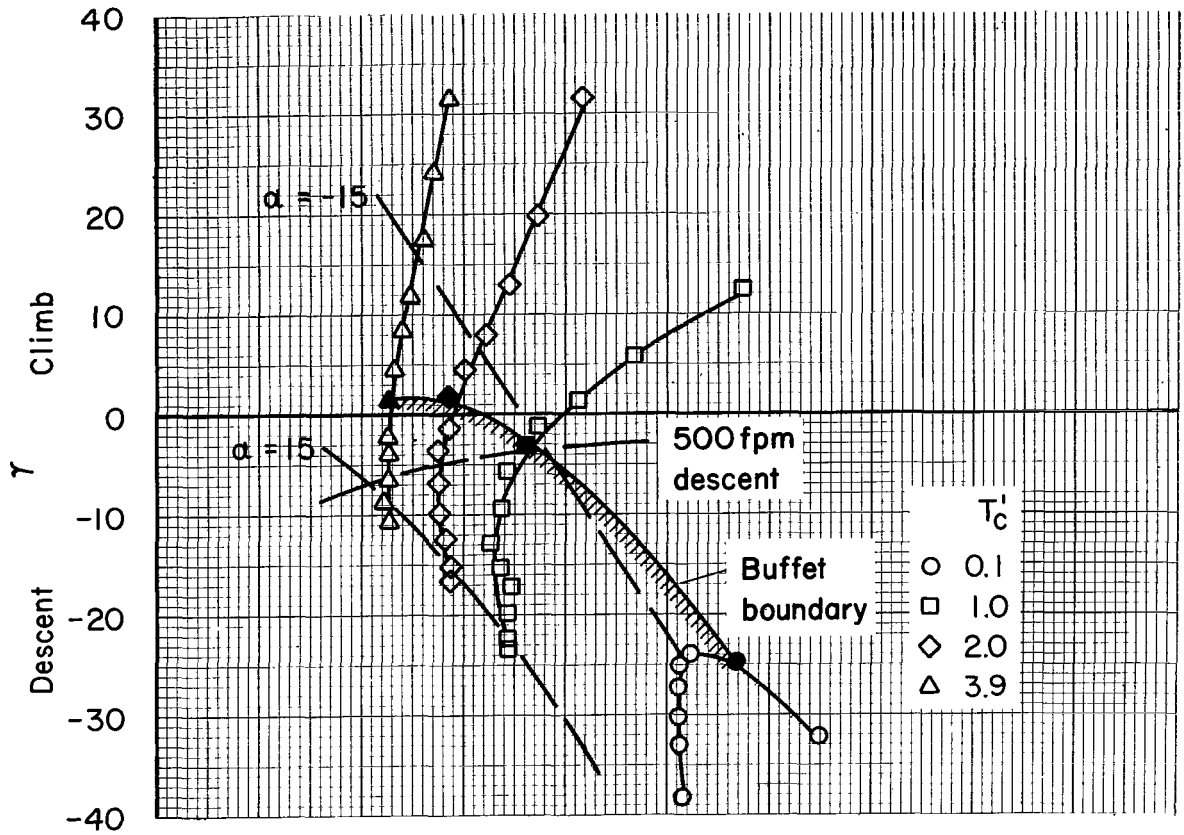
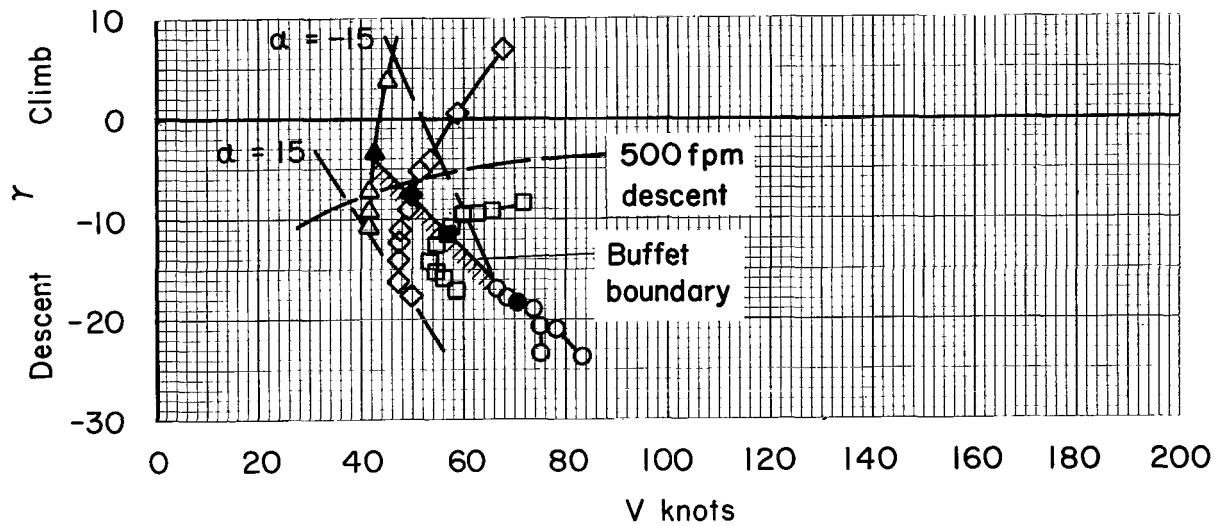


Figure 13.- Variation of fluctuating loads with angle of attack; $\delta_w = 30^\circ$, $\delta_f = 50^\circ$, $C_{\mu_f} = 0.065$.

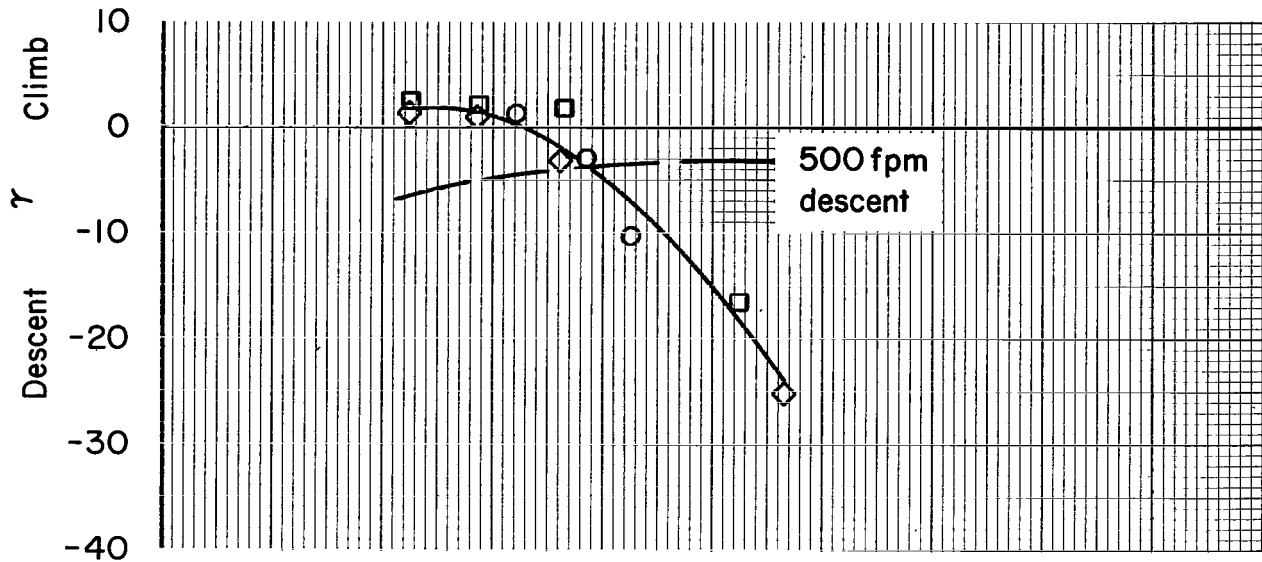


(a) $\delta_w = 0^\circ$, $\delta_f = 30^\circ$, $C_{\mu_f} = 0$, plain wing.

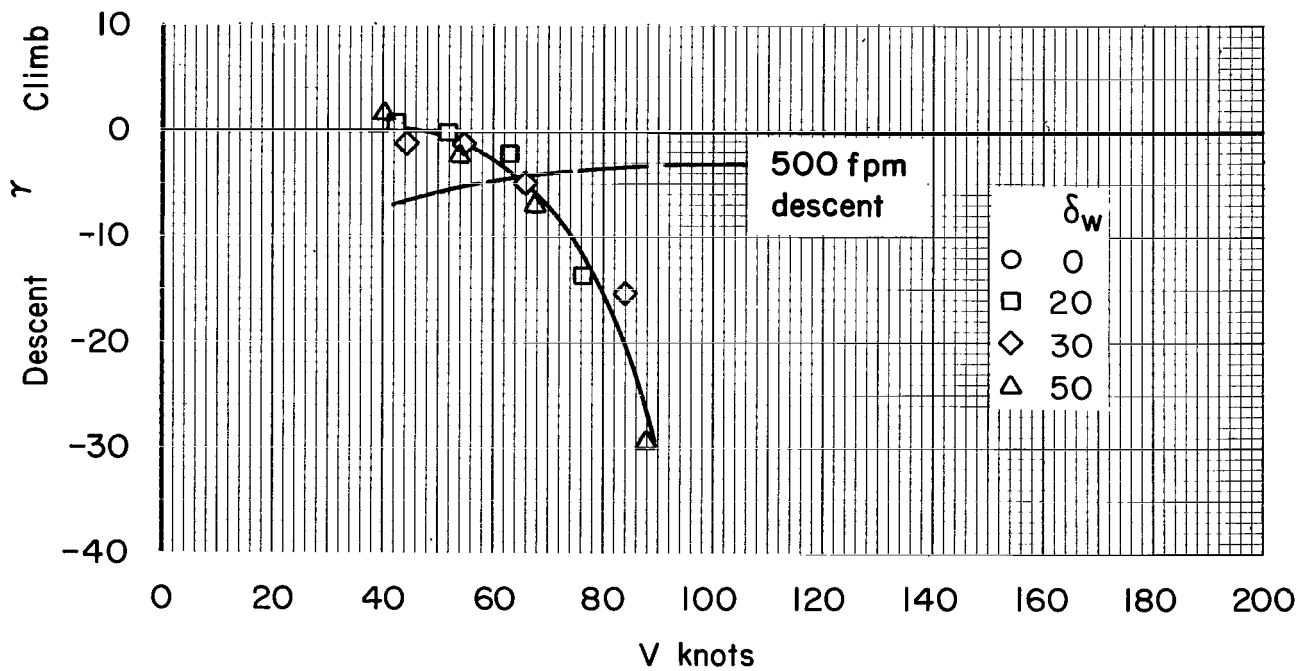


(b) $\delta_w = 30^\circ$, $\delta_f = 50^\circ$, $C_{\mu_f} = 0.065$, BLC nose flap, $C_{\mu_n} = 0.074$.

Figure 14.- Variation of glide angle with forward velocity.

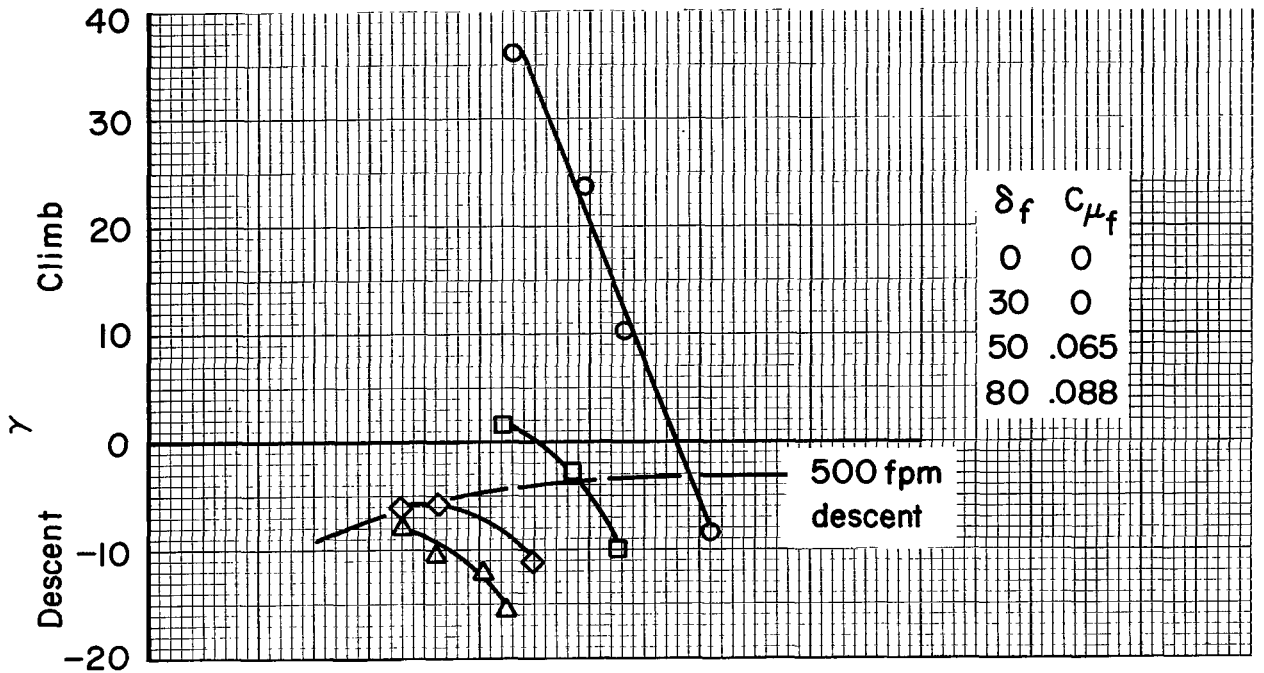


(a) Plain wing.

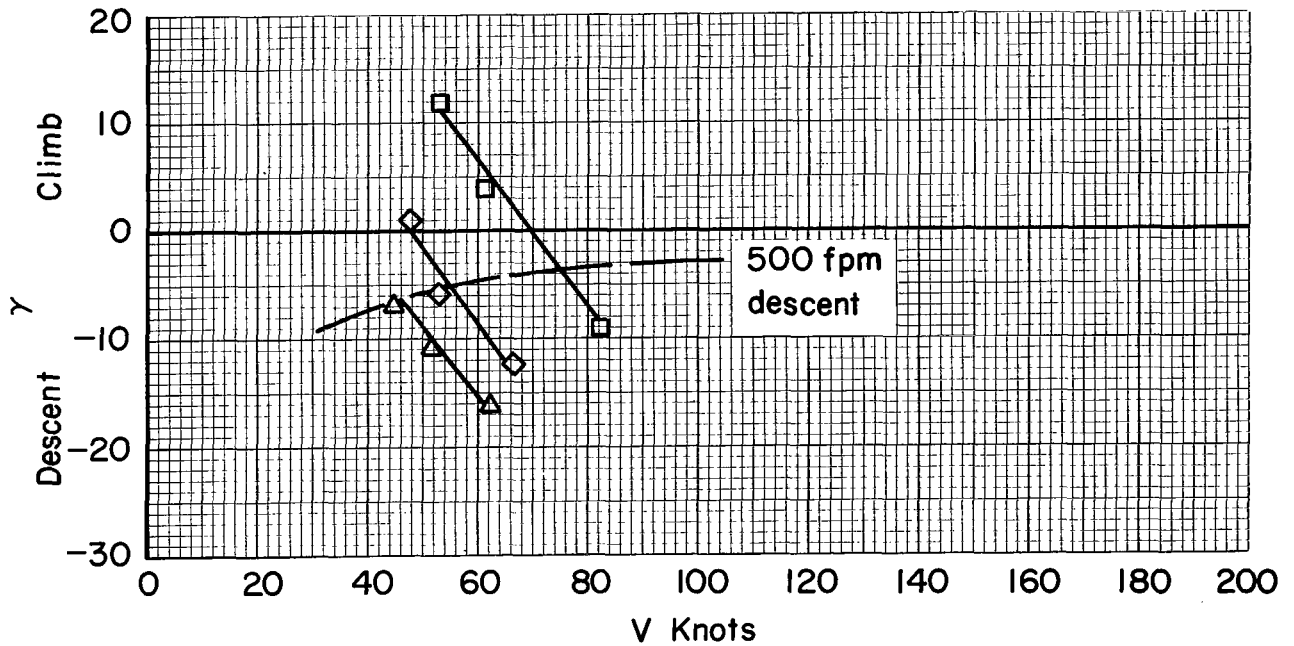


(b) Full-span slat.

Figure 15.- Effect of wing tilt on the stall buffet boundary; $\delta_f = 30^\circ$, $C_{\mu_f} = 0$.

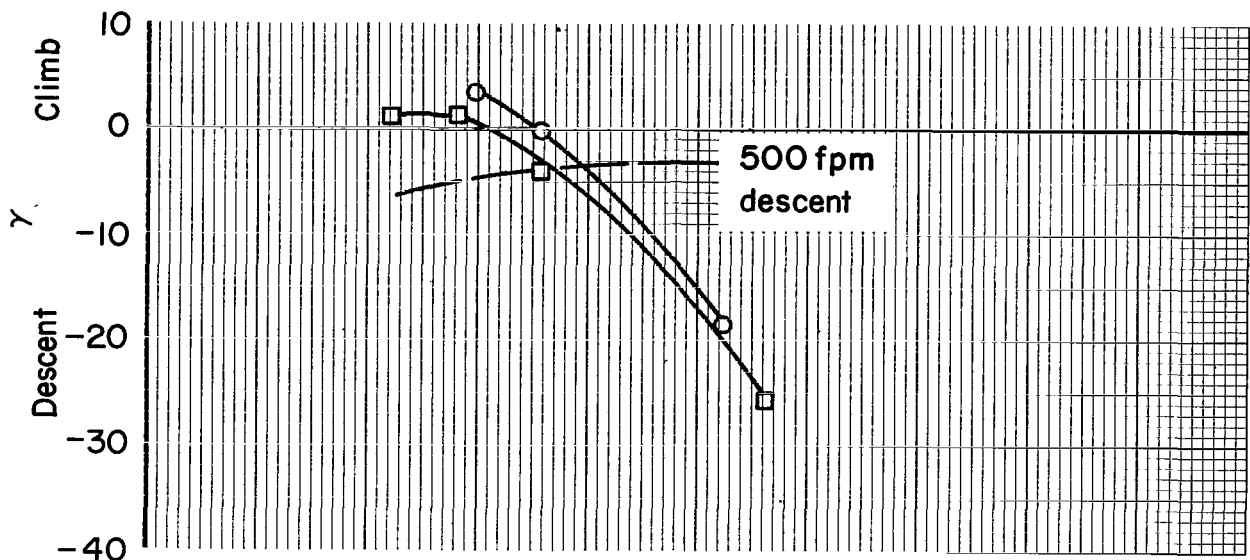


(a) Plain wing

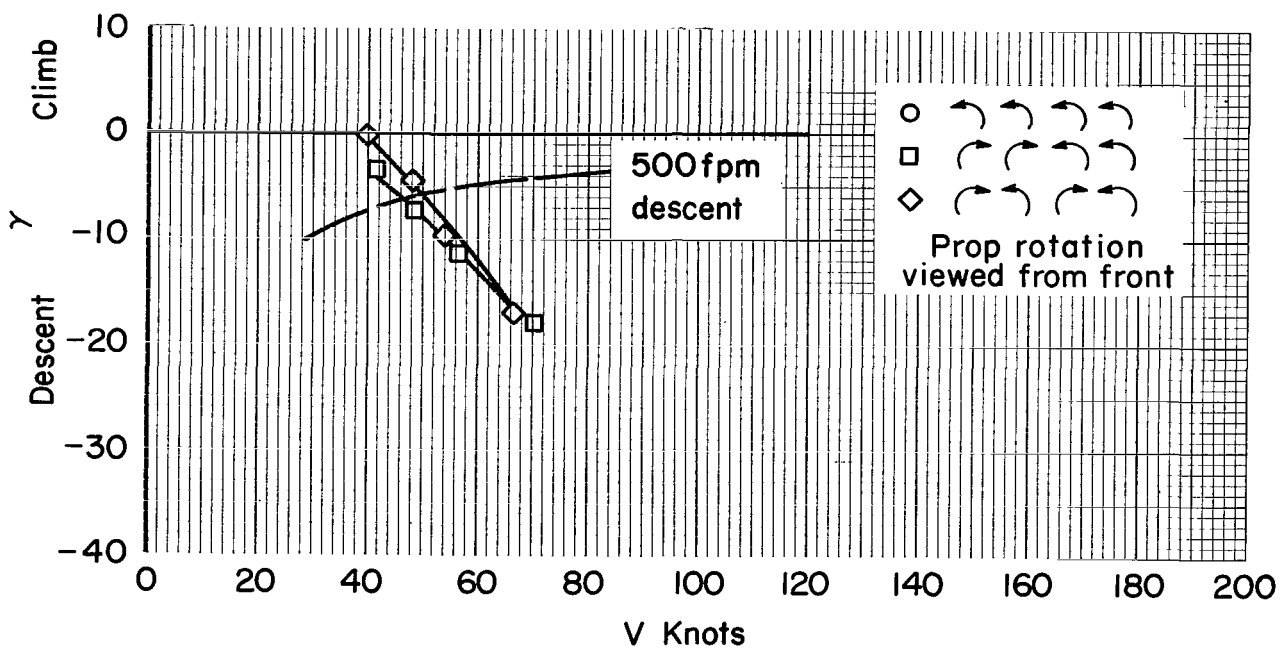


(b) Full-span slat.

Figure 16.- Effect of trailing-edge flap deflection on the stall buffet boundary;
 $\delta_w = 0^\circ$.

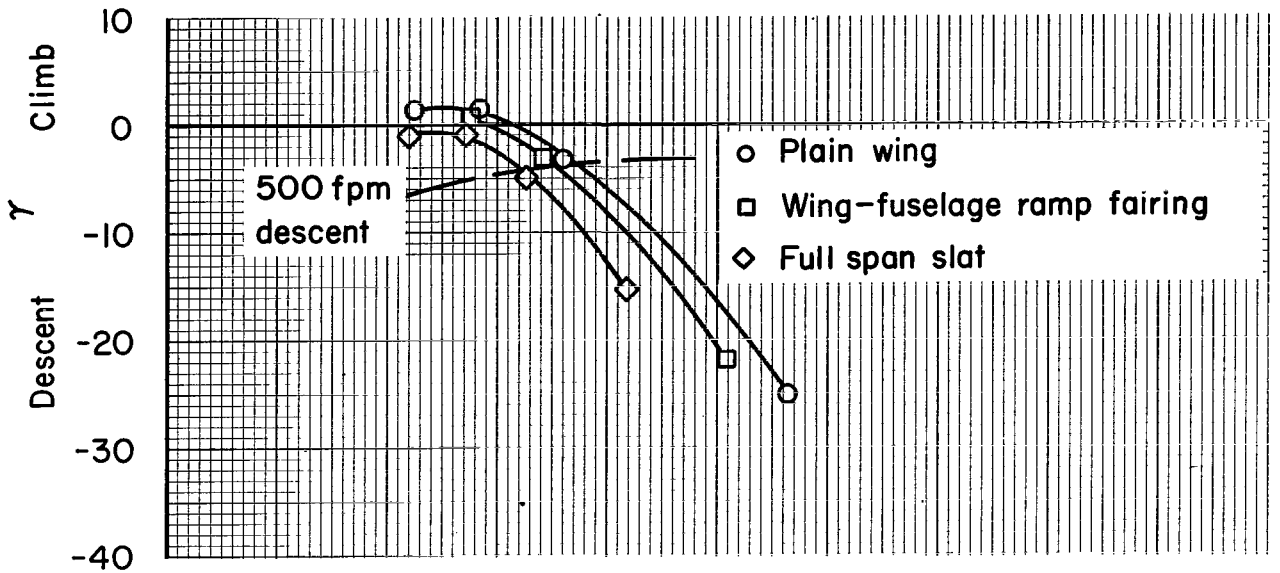


(a) $\delta_f = 30^\circ$, $C_{\mu_f} = 0$

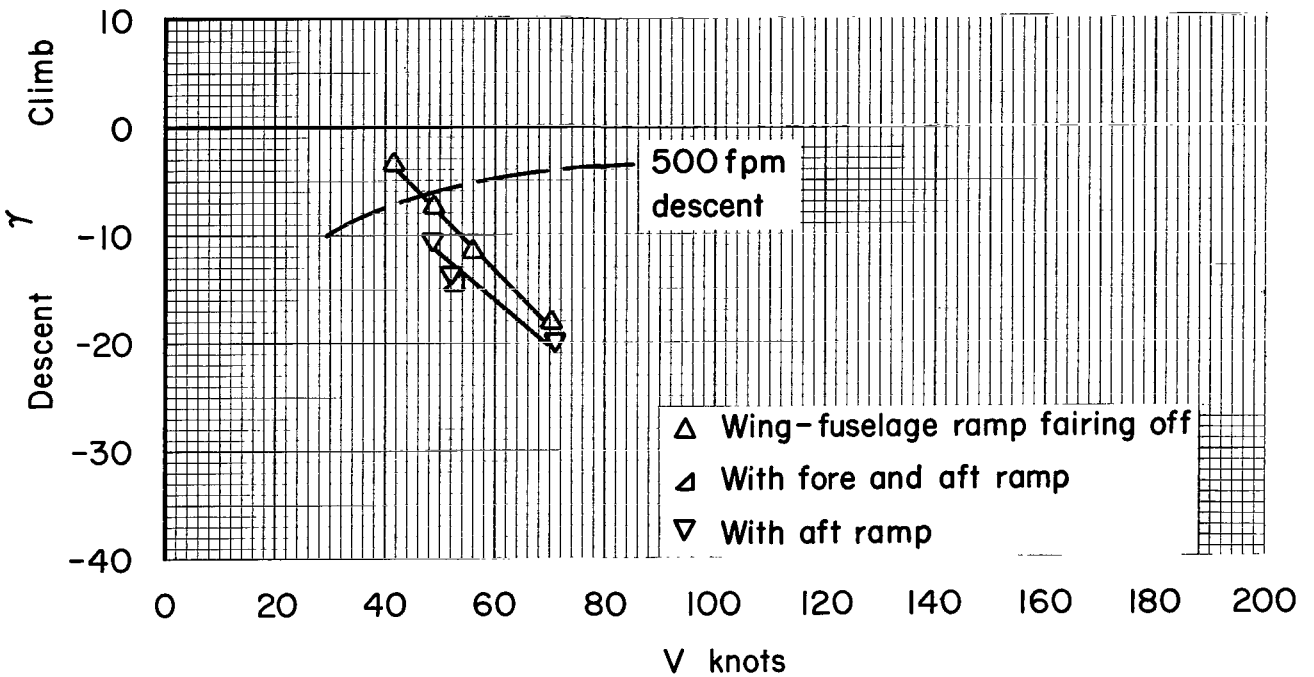


(b) $\delta_f = 50^\circ$, $C_{\mu_f} = 0.065$, BLC nose flap, $C_{\mu_n} = 0.074$.

Figure 17.- Effect of propeller rotation on the stall buffet boundary; $\delta_w = 30^\circ$.



(a) $\delta_f = 30^\circ$, $C_{\mu_f} = 0$



(b) $\delta_f = 50^\circ$, $C_{\mu_f} = 0.065$, BLC nose flap, $C_{\mu_n} = 0.074$.

Figure 18.- Effect of stall control devices on the buffet boundary; $\delta_w = 30^\circ$.

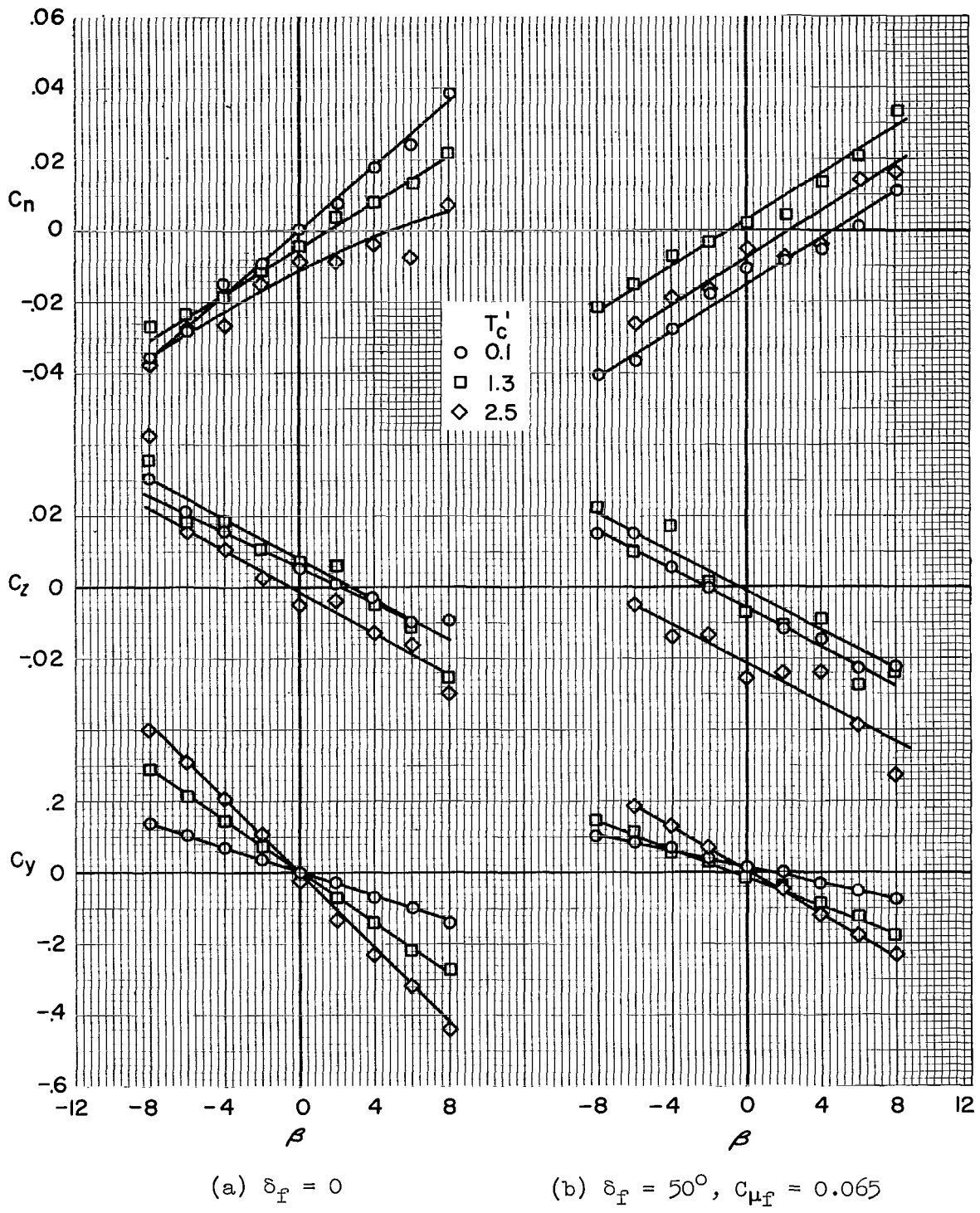


Figure 19.- Lateral and directional characteristics in sideslip; $\delta_w = 0^\circ$, $\alpha = 0^\circ$, $i_t = 14^\circ$, vertical tail on.

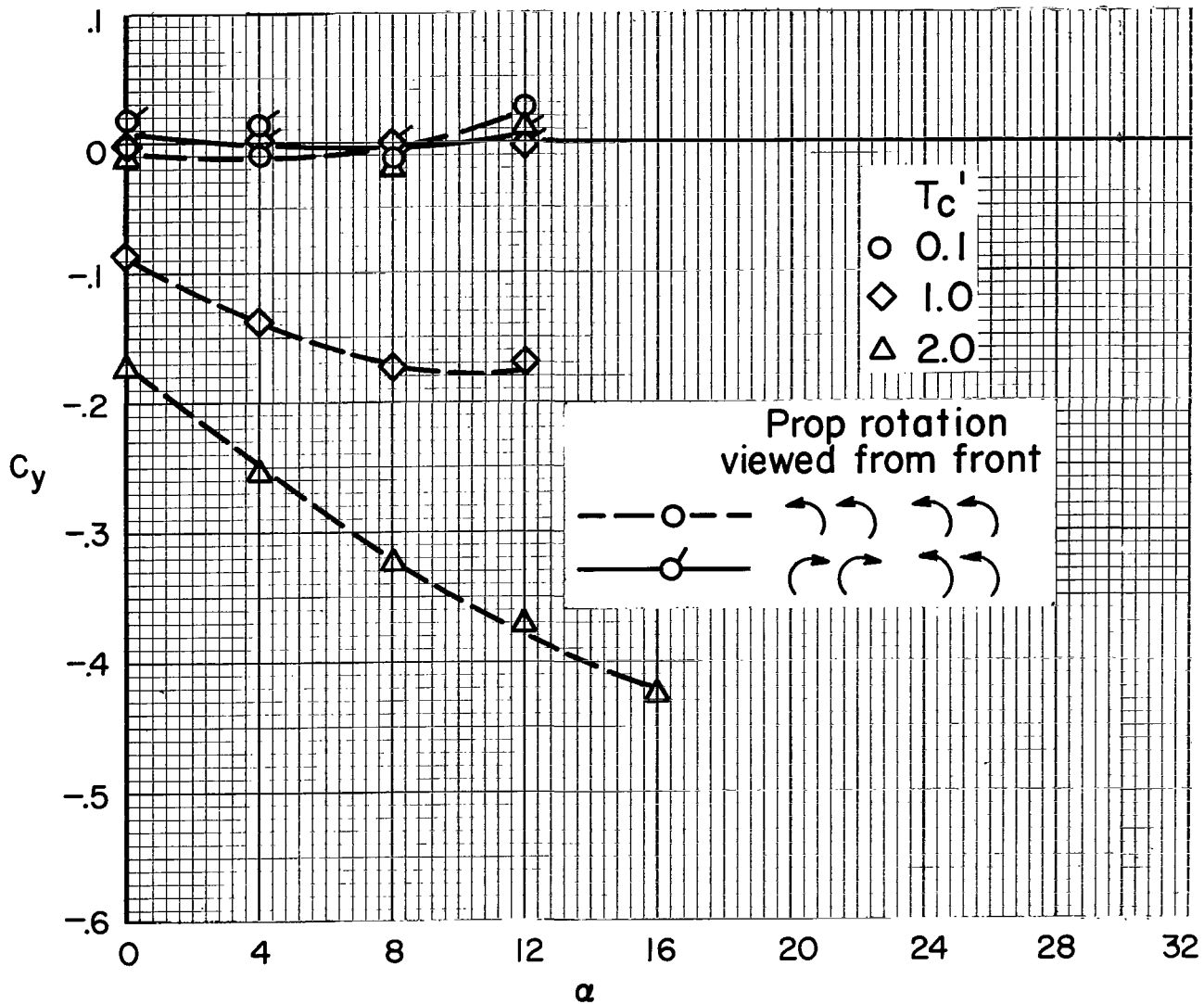


Figure 20.- Effect of propeller rotation on the side-force variation with angle of attack; $\delta_w = 0^\circ$, $\delta_f = 50^\circ$, $C_{\mu f} = 0.065$.